NOX

Electrical Engineering Research Laboratory
The University of Texas
Austin, Texas

Report No. 126 25 May 1962

MICROPULSATION SENSORS WITH LAMINATED MUMETAL CORES

by

Lorimer K. Hill

Francis X. Bostick, Jr.

Contract Nonr 375(14)

NR 371-032/3-27-61

OFFICE OF NAVAL RESEARCH

Washington, D. C.

ELECTRICAL ENGINEERING RESEARCH LABORATORY
THE UNIVERSITY OF TEXAS
Austin, Texas

Report No. 126

25 May 1962

MICROPULSATION SENSORS WITH LAMINATED MUMETAL CORES

by

Lorimer K. Hill

Francis X. Bostick, Jr.

Contract Nonr 375(14)
NR 371-032/3-27-61

OFFICE OF NAVAL RESEARCH
Washington, D. C.

TABLE OF CONTENTS

Table of Contents, cont'd.

LIST OF FIGURES

List of Figures, cont'd.

ABSTRACT

For the past three years the Electrical Engineering Research Laboratory of The University of Texas has been engaged in measuring changes in the earth's magnetic field and earth currents with the sponsorship of the Office of Naval Research under Contracts Nonr 375(01) and Nonr 375(14). In order to supplement the present system for magnetic field measurement using fixed air-cored coils with a portable system for conducting correlation studies, easily transported sensors were needed.

This report contains the derivation and computer solutions of certain equations which specify coils wound on long, straight, ferromagnetic cores. Use of these equations is illustrated in the design of sensors for detecting changes in the earth's magnetic field which occur at frequencies of one cycle per second or less. Design emphasis is placed on wire resistance and completed sensor weight. Included is an account of the construction and testing of three such sensors.

I. INTRODUCTION

Designing a micropulsation sensor having a ferromagnetic core involves two major considerations; namely, the resistance of the winding and the character of the output signal. The direct-current resistance must of course be less than the maximum source resistance that the microvolt amplifier can tolerate. Usually it must be small enough to allow the insertion of a 60-cycle filter between it and the microvolt amplifier. In the particular case considered, the maximum source resistance was 1000 ohms, and the limitation of 500 ohms was placed on the d-c resistance of the winding.

Knowledge of the character of the output signal as a function of ambient field fluctuation is essential if meaningful power spectra and cross-correlation studies are to be made. For all practical purposes the relationship must be linear. The effect of nonlinearities, such as variable permeability, must be made negligible.

One of the objectives in building these coils was mobility of the completed system. Coil weight was therefore a third consideration. An acceptable weight per coil was arbitrarily taken to be about 100 pounds.

The open-circuit sensitivity required was 50 microvolts rms in a uniform field varying sinusoidally with time at a rate of one cycle per second with one gamma peak-to-peak change in flux density.

Design of the coils was accomplished using an equation for the length of wire required to wind a coil of a given shape. For any standard wire diameter,

the coil resistance was readily found by multiplying the wire length by the resistance per unit length tabulated in wire tables. Since a general parabolic shape was considered for the axial cross-section of the coil, the case of the cylindrical type winding of uniform thickness was included. Evaluation of the wire length equation on a digital computer showed that the winding with least resistance was the extreme parabolic, that is, one which tapered on each end to zero thickness. But it was concluded that the practical difficulties in winding such a coil would cause departures from the calculated values far in excess of any hoped for savings.

Although the coil of each sensor was enclosed in an electrostatic shield, protrusion of the core material through each end of this shield allowed capacitive pick-up from surroundings to core to coil. This type of pick-up was minimized by placing each sensor in a completely shielded box.

II. BACKGROUND INFORMATION

A. Resistive Effects in the Winding, A-C and D-C

The problem of designing a coil for sensing micropulsations in the earth's magnetic field requires the consideration of several contributions to the apparent resistance of the coil in order to insure a high unloaded quality factor. The apparent resistance may be considered the sum of several resistive terms, each of which represents a particular cause of power loss when the coil is tuned or loaded, for in both cases current flows in the coil. Since a constant rate of change of flux cannot exist indefinitely, the changes in flux will be assumed alternating, and for simplicity, sinusoidal. Hence, any current flowing in the coil will be assumed sinusoidal.

In considering the various losses it is convenient to use the equivalent circuit of Fig. 1. Within the core are eddy current and hysteresis losses represented by R_e and R_h, respectively. Residual losses[1, 2, 3*] might also be considered. Within the winding are losses caused by skin effect, proximity effect, distributed capacity, and wire resistance, represented respectively by R_s, R_p, R_c, and R.

If the sensor is considered to operate without loading, that is, without external current flow, several factors tend to reduce the sensitivity. Some of these are circulating currents within the L-C_d loop, eddy currents in the winding, eddy currents in the core material, and core hysteresis.

---

* References appear on pages 83-84.

The first three reduce the alternating flux density by producing reverse fields. The last requires excessive magnetizing force in traversing the hysteresis loop.

Since the physical dimensions of the coil are as yet unknown, the only preliminary loss calculation to be made is for skin effect. The increase in resistance at low frequencies due to skin effect can be obtained from the expression [4]

$$\frac{R + R_s}{R} = 1 + \frac{1}{48}\left(\frac{d}{2\delta}\right)^4,$$

where δ = skin depth

$$= \frac{2.60}{\sqrt{f}} \text{ (in), for copper.}$$

Substituting for δ and evaluating at a frequency of one cycle per second for B and S gauge # 22 wire gives

$$\frac{R + R_s}{R} = 1 + 1.17\ (10)^{-11}.$$

The indicated increase in resistance is certainly negligible, and considering the effect of wire diameter, skin effect can be neglected for any wire size of interest.

In that which follows the magnitude of the d-c wire resistance will be emphasized. This does not discount the above mentioned sources of loss as negligible, but rather it provides a definite starting point for the evaluation of sensor designs.

The requirement to be placed on the sensor is that it produce a specified open-circuit voltage for a given rate of change of ambient flux. Design of the sensor is accomplished by finding a satisfactory flux-turn linkage pattern which, of course, will not be unique. Peculiar to each design will be a value of d-c wire resistance together with values of inductance, distributed capacity, and the other loss terms.

B. Factors Influencing the Core Permeability

Consider now the function μ (x) which defines the effective relative permeability at any point x measured axially from the mid-point of the core as shown in Fig. 2c. The value of the apparent permeability at the center of a bar of ferromagnetic material is known to be a function of the dimensions of the bar. For solid, right-circular cylindrical bars, Bozorth and Chapin [5] have drawn curves relating the true permeability of the bar material to the apparent permeability, μ_1, at the middle of the bar, using the length-to-diameter ratio as a parameter. For each value of the parameter there corresponds a maximum value of apparent permeability which is asymptotically approached as the true permeability increases. This maximum value increases as the length-to-diameter ratio is increased until the true permeability of the material is reached. Knowing the minimum true permeability of the material, the maximum length-to-diameter ratio can be selected which will maintain the apparent permeability within

arbitrarily narrow limits, despite increases in true permeability resulting from changing magnetic conditions. Smaller length-to-diameter ratios, although producing greater stability, reduce the apparent permeability.

If a coil is wound on such a bar as outlined in Fig. 2a, those turns of the coil not located at the middle of the bar will realize a core permeability that is less than that at the middle; that is, the voltage induced in any given turn of wire by a fluctuating ambient field will depend upon the position of the turn with respect to the middle of the bar. Bozorth and Chapin investigated this permeability function also. Their conclusions are as follows.[6] The permeability function follows closely the theoretical calculations of Würschmidt[7] (who assumed $\mu = \infty$) and is very nearly parabolic; provided that the true permeability of the material is so high that increasing it will not increase the apparent permeability by more than 10 to 20 per cent for the particular length-to-diameter ratio of interest, and that the magnetizing force is low. The first condition is insured by proper choice of the length-to-diameter ratio. As for the magnetizing force, fluctuations on the order of several micro-oersteds would be typical.[8,9] The shape of the permeability function can be specified by an equation such as the following:

$$\mu(x) = \mu_1 \left[1 - F \left(\frac{x}{\ell} \right)^2 \right] \qquad (1)$$

in which ℓ is the length of the core and F is a dimensionless constant that specifies the permeability near the end of the core. At the end of the core

the function is not parabolic, but begins to approach the value for free space. However, based on the results of Bozorth and Chapin [10] and the suggestion of Block and Rietveld [11], an appropriate value for F is 3.6.

Neglected in the above analysis was the effect of the average value of the earth's magnetic field. If a representative value of the ambient flux density produced by this field is taken to be 25,000 gammas [12], which is equivalent to 0.25 gauss, signals on the order of a few tenths to several gamma would produce minor hysteresis loops as illustrated in Fig. 3. The incremental permeability of these minor loops is the perme ability which must be considered.

The manner in which the incremental permeability of Mumetal laminations changes with signal flux density is suggested by Fig. 4, where the parameter for the various curves is the bias field magnitude. Even though the frequency at which the data were taken was 60 cycles per second, much higher than frequencies of current interest, the data are useful, for they allow a worst case approximation of the incremental permeability, since it decreases somewhat with frequency. After extrapolating the curves to zero alternating flux density, points taken from Fig. 4 were used in plotting Fig. 5. Shown in Fig. 5 is the approximate relationship between incremental permeability and bias field strength. In order to estimate the order of magnitude of the signal flux density and the bias flux density, it will be assumed that the length-to-diameter ratio

chosen for the core and the minimum true permeability of the core material produce an effective permeability of 1000 at the mid-point of the core. The ambient flux density would then be multiplied by 1000 in order to obtain the flux density within the core material. Assuming that the orientation of the core is such that the component of static flux density parallel to the core is 0.25 gauss and that the same component of the micropulsations has a peak-to-peak value of 2.5 gammas, the respective flux densities within the core will be 250 gausses and 0.025 gauss peak-to-peak. From the magnitude of the latter figure it is evident that the curve for $B_\Delta = 0$ in Fig. 5 is representative of the micropulsations. The value of magnetizing force to be used is obtained from the d-c magnetizing curve of Fig. 6 for a flux density of 250 gausses. The dashed line in Fig. 5 represents this magnetizing force. It can be concluded that the static component would have to be more than three times this intensity in order to reduce the incremental permeability below 10,000. Assuming that the incremental permeability is reduced in a manner identical to the reduction in true permeability because of the bar configuation of the core, the effective permeability will be the same for both the bias field and the signal field. Bozorth's curves[13] indicate that a length-to-diameter ratio of 60 would produce an apparent permeability of 1000 if the true permeability were 10,000, and that such apparent permeability would be virtually constant over the range of flux densities encountered.

C. Sources of Spurious Signals and Magnitude Errors

As a possible source of noise, nonlinearities, or spurious signals, the Bàrkhausen effect is the most likely cause. It is the almost discontinuous, stair-step increase in induction for continuous increases in magnetic field intensity. In order to observe the Barkhausen effect, it is necessary that the field change very slowly, a condition which exists in the measurement of micropulsations. Therefore, it is quite probable that high frequency components not present in the ambient field will appear in the data because of discontinuous jumps between levels of magnetization. Although it has been demonstrated that the greatest Barkhausen noise power exists in or above the region of greatest slope on the hysteresis loop, the noise is measurable in low fields [14]. Latimer [15] even suggests that hysteresis loops in low fields are composed of closed stair-step functions, although he concedes that the averaging over large volumes may preclude nonlinearity. Bozorth [16] states that the noise is proportional to the number of longitudinal subdivisions of the core material. This means that lamination of the core would intensify such noise.

Mechanical vibrations caused by sound or earth motions in the vicinity of the sensors could produce two erroneous signals simultaneously. One would result from mechanical stressing of the core material and consequent change in induction [17]. A second would result from physical motion of the sensor in the earth's field. This latter effect may be appreciable because of the large magnitude of the constant field.

III. WIRE RESISTANCE AND WIRE LENGTH

A. Wire Length as a Function of Parameters Defining Coil Shape

The length of wire which can be wound into a coil of specified dimensions can be expressed analytically by the equation

$$\phi = \phi_A + \frac{4\pi}{K_1 K_2 d^2} \int_o^C [1/2\, f^2(x) + r_1 f(x)]\, dx, \qquad (2)$$

where K_1, K_2 are wire spacing factors,

d is the wire diameter (bare),

r_1 is the coil form radius,

C is the length of one-half of the winding,

f (x) is the thickness of the winding at the distance x measured axially from the center of the coil,

ϕ_A is the additional wire length required to connect turns and layers.

This equation is derived in Appendix A. In order to simplify that which follows, the quantity ϕ_A, which accounts for the departure of the turns from plane rings and the possibility of having some layers shorter than others, is neglected as being much smaller than the second term of the above expression. The axial shape of the coil is now arbitrarily taken to be parabolic; that is, a section taken along the axis of the coil would have an outline described by a parabola symmetrical about the axial center of

the coil. This shape is expressed by the following equation

$$f(x) = H\left[1 - J\left(\frac{x}{C}\right)^2\right], \tag{3}$$

in which the quantity H is the thickness of the coil at the center and the dimensionless quantity J determines the thickness of the coil on the ends. Eqs. (2) and (3) together imply a definite length of wire corresponding to any set of values for H, J, and C; provided that $K_1 K_2 d^2$ and r_1 are fixed. The resistance of the wire is simply the wire length multiplied by a constant. Use of the wire diameter d as a parameter is convenient since a standard wire size will probably be chosen.

If it is now demanded that the coil produce a specified, open-circuit output voltage for given ambient field conditions and for a given core of permeability $\mu(x)$, the three variables H, J, and C can be reduced to two. The equation which contains the necessary restriction is

$$K_1 K_2 d^2 K' = \int_0^C f(x)\,\mu(x)\,dx. \tag{4}$$

This equation is derived in Appendix A. The quantity K' is dimensionless and given by

$$K' = \frac{E}{\sqrt{2}\,\omega\,\mu_o H_o A}, \tag{5}$$

where E = rms open-circuit output voltage,

ω = radian frequency of sinusoidally varying ambient field,

μ_o = permeability of free space,

H_o = peak value of ambient field,

A = area of core material.

If the permeability of the core is assumed to decrease parabolically from the center of the core toward the ends, as expressed by Eq. (1), Appendix B shows that substitution of Eqs. (1) and (3) into Eqs. (2) and (4) yields

$$\frac{K_1 K_2 d^2 \sqrt{F}\ \phi}{4\pi \ell r_1^2} = H' Z \left[\frac{H'}{2}\left(1 - \frac{2}{3}J + \frac{J^2}{5}\right) + \left(1 - \frac{J}{3}\right)\right] \qquad (6)$$

and

$$\frac{K_1 K_2 d^2 \sqrt{F}}{\ell r_1}\left(\frac{K'}{\mu_1}\right) = H' Z\left[\left(1 - \frac{Z^2}{3}\right) - J\left(\frac{1}{3} - \frac{Z^2}{5}\right)\right] \qquad (7)$$

where

$$H' = \frac{H}{r_1},$$

$$Z = \sqrt{F}\left(\frac{C}{\ell}\right).$$

The right-hand sides of these equations are combinations of dimensionless variables. The left-hand sides of Eqs. (6) and (7) can be represented by, respectively, quantities ϕ_1 and ϕ_2; thus,

$$\phi_1 = H'Z\left[\frac{H'}{2}(1 - \frac{2}{3}J + \frac{J^2}{5}) + (1 - \frac{J}{3})\right] \tag{8a}$$

and

$$\phi_2 = H'Z\left[(1 - \frac{Z^2}{3}) - J(\frac{1}{3} - \frac{Z^2}{5})\right]. \tag{8b}$$

Eqs. (8) imply that ϕ_1 is a function of two independent variables and the parameter ϕ_2. Noting that H' cannot produce a minimum value of ϕ_1, it is eliminated. The remaining variables, ϕ_1, Z, and J, can be considered to form a three-dimensional space in which there exists a family of surfaces, each corresponding to a value of ϕ_2.

At this point it is important to note that the wire length ϕ differs from the quantity ϕ_1 by a constant, for various value of ϕ_2, only when ϕ_2 is changed by a factor such as output voltage E, not common to ϕ_1. This somewhat limits the usefulness at ϕ_2 as a parameter; however, some useful information is later obtained from it.

Eq. (7) also provides some information about the relative coil length which will be useful in determining the dimensions of the coil. If the number of layers in the center of the coil is denoted by λ, the thickness in the center is

$$H = K_1 d\lambda$$

and the relative thickness is

$$H' = \frac{H}{r_1} = \frac{K_1 d\lambda}{r_1} .$$

Dividing both sides of Eq. (7) by this last expression for H' yields

$$Z\left[\left(1 - \frac{Z^2}{3}\right) - J\left(\frac{1}{3} - \frac{Z^2}{5}\right)\right] = \frac{K_2 d\sqrt{F}}{\ell\lambda}\left(\frac{K'}{\mu_1}\right), \tag{9}$$

an implicit equation for Z as a function of the axial spacing factor K_2 and the number of layers in the center of the coil.

B. Computer Solution for Resistance

If the solution of Eq. (7) for H' is substituted into Eq. (6), the wire length becomes

$$\phi = \frac{2\pi\sqrt{F}}{\ell}\left(\frac{K'}{\mu_1}\right)^2 K_1 K_2 d^2 \frac{\left(1 - \frac{2}{3}J + \frac{J^2}{5}\right)}{Z\left[\left(1 - \frac{Z^2}{3}\right) - J\left(\frac{1}{3} - \frac{Z^2}{5}\right)\right]^2}$$

$$+ 4\pi r_1 \left(\frac{K'}{\mu_1}\right) \frac{\left(1 - \frac{J}{3}\right)}{\left[\left(1 - \frac{Z^2}{3}\right) - J\left(\frac{1}{3} - \frac{Z^2}{5}\right)\right]} . \tag{10}$$

This equation and some interesting relations contained in it are shown in Appendix B. But rather than take the partial derivatives with respect to Z and J in order to find the minima, if one or more exist, it is more informative to evaluate the wire length ϕ, or a quantity such a ϕ_1 which represents ϕ, for several values of Z and J within the range of interest. In this manner a firm representation of the wire length function can be obtained.

Eqs. (8) were chosen to be programmed for solution by a digital computer. Three sets of solutions were obtained, each set corresponding to a particular value of ϕ_2. Although these values were not arbitrarily picked, but correspond to certain conditions peculiar to this application, interpretation of the results in terms of ϕ_2 need not be so limited, because ϕ_2 and ϕ_1 are both dimensionless. Since it may be desirable to change some of the components of φ_2 in order to see how the solution is effected, the values used are as follows:

$$K_1K_2 = 1.25$$

$$d = \frac{0.0253}{12} \text{ (feet), \#22 B \& S gauge}$$

$$F = 3.6$$

$$r_1 = \frac{\ell}{64} \text{ (feet), } \ell \text{ in feet,}$$

$$\frac{K'}{\mu_1} = \frac{4.845\,(10)^5}{\ell^2}, \ \ell \text{ in feet}$$

where

$$E = 5(10)^{-5} \text{ (volts), rms,}$$

$$\omega = 2\pi \frac{\text{(radians)}}{\text{(second)}},$$

$$\mu_o H_o = 1.0 \text{ (gamma), peak-to-peak}$$

$$= 5(10)^{-6} \text{ (gauss), peak,}$$

$$= 5(10)^{-10} \frac{\text{(webers)}}{\text{(meter)}^2}, \text{ peak,}$$

$$A = 2.323(10)^{-5}\,\ell^2 \text{ (meters)}^2, \ \ell \text{ in feet.}$$

The coil form radius and the core material area have been made functions of core length for convenience (see Section IV). The expression for ϕ_2 is

$$\phi_2 = \frac{K_1 K_2 d^2 \sqrt{F}}{\ell r_1} \left(\frac{K'}{\mu_1}\right),$$

which upon substitution of the above values becomes

$$\phi_2 = \frac{3.269(10)^2}{\ell^4}, \ \ell \text{ in feet.}$$

Evaluation of ϕ_2 for core lengths of 5, 6, and 10 feet gives 0.5231, 0.2523, and 0.03269, respectively.

One important result is that a minimum of ϕ_1 as a function of Z exists over a wide range of values of ϕ_2 within the interval $0 \leq J \leq 1$. This is illustrated in Figs. 7 and 8. Fig. 7 shows that the minimum occurs at smaller values of Z and becomes less pronounced as ϕ_2 is decreased; however, the value of ϕ_1 for constant values of Z and J is parabolic with ϕ_2, the same as it is with H'.

The effect of decreasing the thickness of the coil on the ends, by winding it in a parabolic shape, is shown in Fig. 8 where $\phi_2 = 0.2523$. It can be seen that, although the minimum resistance of the coil, or the length of wire required to wind the coil, decreases continually from a cylindrical shape (J = 0.0) to a parabolic shape with zero thickness on the ends (J=1.0), the minimum resistance or wire length for a cylindrical coil is not even two per cent greater than the lowest obtainable. But the advantage of winding a coil in a parabolic shape becomes greater as the coil is extended toward the ends of the core. The reverse is true for short coils (small Z) which may require more wire in a parabolic shape than in a cylindrical shape

because of rapid increase in radius of the outer turns as the coil is shortened. In this latter case there is a minimum as a function of J for constant Z which is quite evident at Z = 0.490. At this point ϕ_1 is the same for the cylindrical winding as it is for the fully parabolic, but intermediate shapes can be wound with less wire.

Fig. 9 shows several contours of constant resistance projected on the J-Z plane. The values of these contours are based on the estimated minimum of ϕ_1 at J = 1.0 as read from Fig. 8.

Fig. 10 shows the value of Z which must be used in order to obtain minimum resistance in a cylindrical coil for a given value of ϕ_2. Also indicated are the approximate boundaries of the region in which the resistance is within ten per cent of the minimum.

C. Additional Considerations

Because of the simplicity of winding a cylindrical coil, departure from this shape should not be attempted without due consideration of what is to be gained. In Fig. 11 are shown three curves of ϕ_1 versus Z. Also shown are several lines of constant coil thickness, H'. For H' = 0.55 it can be seen that the wire length is the same for the parabolic coil (J = 1.0) as it is for the cylindrical coil; the only difference is that the parabolic coil is longer (Z = 0.785, rather than 0.500).

If coil thickness is important because of peculiarities in the enclosure, the cylindrical coil offers the only solution. This can be seen in

Figs. 12 and 13, but Fig. 11 indicates that in order to wind a long thin coil, an excessive amount of wire is required.

The greatest theoretical advantage of using a parabolic winding for the purpose of reducing the coil resistance is found in coils which must, for some reason, extend over almost the entire length of the core. Here a decrease of ten per cent or more from that of a cylindrical coil of the same length may be realized, although a shorter, cylindrical coil may have the same resistance, or even less, and also be thinner in the center.

For any coil shape including cylindrical, an approximation to the desired shape must be made. With reference to a cylindrical coil, this implies the highly probable case of a fractional outer layer, the remedy for which is a slight adjustment of the coil length, or the use of more or less wire which changes the induced voltage. A parabolic coil requires the exact location of the last turn on each layer. Even though a theoretically good approximation to the desired shape may be made by the calculated envelope of the coil, the accuracy obtainable in practice depends on the spacing between turns.

Assuming that the winding of a coil shape to obtain, perhaps, a two per cent reduction in wire resistance from that of a cylindrical coil presents no practical difficulties, an estimated parameter, the permeability of a laminated core, may cause such small gain to be entirely obscured because of error in the estimation. Some of the variables involved in determining the permeability of a laminated core are undoubtedly the thickness of

the laminations, the stacking factor, and the cross-sectional shape of the stack. The results presented by Bozorth and Chapin[18] for the variation of the permeability along bars of simple cylindrical shape seem to imply that useful information about laminated bars must be empirically obtained. Because of the lack of such information, the possible savings pronounced above may be purely academic. However, the nature of the solution must remain: that there is an optimum length and shape for a coil wound on a long straight core.

If the above results are taken to be valid, it might be argued that the calculated savings are negligible in an actual circuit, where savings must be measured in decibels, rather than in per cent. Taking as an example an untuned coil with wire resistance of 500 ohms feeding as amplifier with input inpedance of 100,000 ohms, a ten per cent change in coil resistance has an immeasurably small effect on the signal voltage. Whereas in a similar tuned coil the effect on the circuit quality factor and on the response would be much more pronounced. This latter situation, however, demands knowledge of the proximity of the self-resonant frequency to the frequency band of interest. And in this connection the flexibility of the formulas (specifically, the inclusion of terms accounting for wire spacing) should allow a compromise between coil resistance and distributed capacity, assuming that a valid expression for the distributed capacity in terms of coil dimensions can be found.

Cost is another item of interest. The savings in wire could be more than nullified by the meticulous design and fabrication techniques required in winding a coil shape other than cylindrical.

The conclusion is that the advantages of winding a coil of shape other than cylindrical do not warrant such an undertaking, provided a cylindrical coil of nearly optimum length can be placed on the core.

IV. COIL DESIGN

A. Selection of Wire Size and Core Length Using Weight and Resistance as Criteria.

In order to reduce the number of variables which must be considered in designing an iron-cored coil, a fixed length-to-diameter ratio will be assumed for the core.

$$\frac{\ell}{D} = \text{constant}$$

This implies a constant effective permeability, μ_1, at the center of the bar's length if the true permeability of the material is known. If the bar is not of circular cross-section, it will be assumed that a value for D can be found as a function of the actual core material cross-section.

$$D = D(A)$$

The area of the core is then a function of the core length.

$$A = A(\ell)$$

For given field and output conditions

$$K' = \frac{E}{\sqrt{2}\,\omega\, H_o \mu_o A}$$

becomes

$$K' = K'(\ell)$$

The outside radius of the coil form, r_1, is found for a specific core length, insuring that it will provide area for the core, coil form, and

material affording mechanical stability. The ratio of radius to core length is maintained constant thereafter.

$$\frac{\ell}{r_1} = \text{constant}$$

If the final evaluation of ℓ implies a radius that is not readily obtained, further calculations can be made using the nearest value of radius of the material available for the coil form.

Before incorporating the above simplifications in Eq. (B.12a), which is repeated here,

$$\phi = m_1(K_1K_2d^2) + b_1,$$

where

$$m_1 = \frac{2\pi\sqrt{F}}{\ell}\left(\frac{K'}{\mu_1}\right)^2 \frac{(1 - \frac{2}{3}J + \frac{J^2}{5})}{Z\left[(1 - \frac{Z^2}{3}) - J(\frac{1}{3} - \frac{Z^2}{5})\right]^2},$$

$$b_1 = 4\pi r_1\left(\frac{K'}{\mu_1}\right) \frac{1 - \frac{J}{3}}{\left[(1 - \frac{Z^2}{3}) - J(\frac{1}{3} - \frac{Z^2}{5})\right]}, \qquad (11)$$

use will be made of the results of the attempt to minimize the wire length and hence the wire resistance. Values for J and Z are picked which will produce a value of resistance very near the smallest value obtainable. Such values can be the easily handled numbers

$$J = 0, \text{ (for a cylindrical winding)}$$

and

$$Z = 0.5.$$

Substituting these into Eq. (IV.1),

$$\phi = m_1(K_1K_2d^2) + b_1,$$

where

$$m_1 = \frac{36\pi\sqrt{F}}{(2.75)^2\ell}\left(\frac{K'}{\mu_1}\right)^2,$$

$$b_1 = \frac{12\pi r_1}{2.75}\left(\frac{K'}{\mu_1}\right). \qquad (12)$$

Use of the simplifications is illustrated in the following. For sinusoidal fluctuations in the ambient flux density of one gamma peak-to-peak at one cycle per second, let the required output voltage be 50 microvolts, rms. Assume that the dimension D for a laminated core of square cross-section is the length of a side of the square; that is to say that the equivalent diameter, for the purpose of determining the length-to-diameter ratio of the core, is the diameter of the inscribed circle. The area of the core is then

$$A = sD^2$$

where s is the stacking factor for the core. The length-to-diameter ratio will be chosen as

$$\frac{\ell}{D} = 60.$$

This implies a permeability at the center of the bar of

$$\mu_1 = 1000$$

for a true permeability of 10,000.[19] The area can now be written as

$$A = \frac{s\ell^2}{3600} .$$

The ratio $\frac{K'}{\mu_1}$ which appears in Eq. (12) can now be written in terms of the length of the bar,

$$\frac{K'}{\mu_1} = \frac{4.845(10)^5}{\ell^2} \text{ (dimensionless)},$$

where ℓ is in feet and s is assumed to be 0.90.

For evaluation of the coil form radius r_1 in terms of the core length ℓ, let the coil form have a thickness

$$t = 0.25 \text{ (inch)}$$

for

$$\ell = 6.00 \text{ (feet)}.$$

Fig. 14 shows that the minimum r_1 which will contain both the coil form and the core must be

$$r_1 = t + \frac{D}{\sqrt{2}}$$

$$r_1 = 0.25 + \frac{1.2}{\sqrt{2}}$$

$$r_1 = 1.0984 \text{ (inches)}.$$

Since a standard tubing size has an outside radius slightly larger than this value, namely, 1.125 (inches), the larger value will be used for r_1. The ratio of core length to coil form radius is now fixed.

$$\frac{\ell}{r_1} = \frac{72.0}{1.125} = 64.0$$

If the value of the constant F is taken as 3.6, as discussed above, Eq. (12 becomes

$$\phi = \frac{4.626(10)^{10}}{\ell^5}(K_1K_2d^2) + \frac{1.038(10)^5}{\ell}, \qquad (13)$$

where d is in inches,

ℓ is in feet,

ϕ is in feet.

Fig. 15 shows wire length as a function of $K_1K_2d^2$ with core length as a parameter. Indicated on the abscissa are the values of $K_1K_2d^2$ which correspond to various sizes of wire covered with double formvar.[20] These values do not include a tolerance for spacing between turns, but only the insulation thickness. This plot vividly illustrates the effect of core length on wire length.

Figure 16 shows the manner in which the wire resistance and wire weight vary with wire gauge number for three core lengths: five, six and ten feet. A representative value of the product K_1K_2 has been taken to be 1.25, for it can be easily adjusted after the wire diameter and core length have been fixed. It will be noted that the use of $Z = 0.5$ in the construction of Fig. 16 implies an optimum coil shape for only one value of the ratio of the square of the wire diameter to the core length. For if this ratio is maintained constant, ϕ_2 is also constant. In Fig. 16 ϕ_2 is not constant, but ranges from 0.013 to 2.1. These extreme values occur for #26 wire on a 10-foot core and #16 wire on a 5-foot core, respectively. The error in the resistance at these

points is about five per cent. This error is insignificant compared to the magnitude of the change in resistance over the range of wire sizes considered.

As an aid in selecting the core length and wire diameter, the weight of the core material should be known. The above-mentioned relationship between core length and core area, when multiplied by core length, gives the volume of core material.

$$\text{Core Material Volume} = \frac{s\ell^3}{36} \text{ (inches)}^3,$$

where ℓ is in inches.

Choosing $s = 0.9$, as before, and using the value 0.307 pounds per cubic inch as the density[21] of Mumetal,

$$\text{Core Weight, } W_c = 0.1326\,\ell^3 \text{ (pounds)},$$

where ℓ is in feet.

The three values of core weight are shown on Fig. 16.

For this particular application a core length of six feet was chosen to be used with a wire size of #22 B & S gauge. Tentatively, the values for wire length, resistance, and weight, and core weight are

$$\phi = 22,060 \text{ (feet)},$$

$$R = 356.0 \text{ (ohms)},$$

$$W = 42.91 \text{ (pounds)},$$

$$W_c = 28.64 \text{ (pounds)}.$$

The total weight of wire and core is about 72 pounds. Allowing for weight of

the coil form and rigid packing of the core to prevent bending, the total weight could be about 90 pounds.

B. Specification of Coil Dimensions.

Having decided on the core length and wire size, the coil length, 2C, and the number of layers in the coil must be found using estimates of the spacing factors K_1 and K_2. Theoretically, the coil can then be wound to fill the space allotted on the coil form without regard for the number of turns, since they are involved implicitly.

In deciding on the number of layers, it is helpful to know the location of the terminals and whether or not the coil is to be wound on the form in one solid piece. Because of convenience in connecting a cable to the terminals, it was decided to place them together at one end of the coil. Splitting the coil into sections is advantageous electrically because of the reduction in distributed capacity. A constructional advantage is also gained if a waterproofing compound is applied while the coil is being wound, for winding can be stopped after completion of a section without danger of the compound hardening where additional wire is to be wound. Sectionizing the coil implies an odd number of layers in the coil, if the wire leaving a section is to go directly into the next section. For section separators very narrow compared to the overall length of the coil it will be assumed that the winding length can be the same as if no separators were used, without reducing the sensitivity of the coil by moving it toward the low permeability ends of the core. Design of the coil will therefore proceed as if it were to be wound in one section with an odd number of layers.

Fig. 9 shows that for Z in the interval $(0.44, 0.56)$ the resistance of a cylindrical winding will be less than two per cent above the lowest resistance obtainable in a parabolic winding. Although the spacing factor product used in obtaining the computer solution was $K_1K_2 = 1.25$, Fig. 10 shows that a small change in this product will have little effect on the value of Z at which a minimum occurs for a cylindrical coil. Since the length of the coil is independent of the radial spacing factor K_1 (see Sec. III. A), K_2 is the only factor which must be estimated in finding the coil length. The spacing factor due to insulation alone on #22 Nyclad is the ratio of coated diameter to bare diameter,

$$K_2 = \frac{0.0266}{0.0253} = 1.051.$$

In order to allow for nonuniformity in winding and separation of turns by the waterproofing compound, an additional spacing of one and one-half times the insulation spacing was used. K_2 is then

$$K_2 = 1.051 + 0.077 = 1.128.$$

Repeating here the equation for Z,

$$Z\left[\left(1 - \frac{Z^2}{3}\right) - J\left(\frac{1}{3} - \frac{Z^2}{5}\right)\right] = \frac{K_2 d\sqrt{F}}{\ell\lambda}\left(\frac{K'}{\mu_1}\right),$$

the equation for a cylindrical coil with $J = 0$ is

$$Z\left(1 - \frac{Z^2}{3}\right) = \frac{K_2 d\sqrt{F}}{\ell\lambda}\left(\frac{K'}{\mu_1}\right). \tag{14}$$

The left-hand side of this equation is plotted as a function of Z in Fig. 17

so that the equation may be readily solved. The right-hand side is now evaluated:

$$\frac{K_2 d\sqrt{F}}{\ell\lambda}\left(\frac{K'}{\mu_1}\right) = \frac{10.123}{\lambda},$$

where

$K_2 = 1.128$

$d = 0.0253$ (in)

$F = 3.6$

$\frac{K'}{\mu_1} = 1.346(10)^4$

$\ell = 72$ (in).

Table 1 shows the values used to obtain Z from Fig. 17. The total length of the winding was found by

$$2C = \frac{2\ell}{\sqrt{F}} Z$$

$$2C = 75.89Z \text{ (in)}.$$

Without paper or other stiff insulation between layers, each turn will lie in a groove formed by the turns in the next lower layer. But turns of adjacent layers must cross at some point, and the spacing at the cross-over point cannot be less than wire insulation. Therefore, the product $K_1 d$ was taken as the coated diameter of the wire. The thickness in Table 1 was calculated using

$$H = K_1 d\lambda$$

$$H = 0.0266\lambda \text{ (in)},$$

where $K_1 = 1.051$

$d = 0.0253$ (in).

Table 1

No. of Layers λ	$\frac{10.123}{\lambda}$	Z (Fig. 17)	2C (in)	H (in)
19	0.5328	0.608	46.1	0.505
20	0.5062	0.566	43.0	0.532
21	0.4820	0.532	40.4	0.559
22	0.4601	0.502	38.1	0.585
23	0.4401	0.476	36.1	0.612
24	0.4218	0.453	34.4	0.638
25	0.4049	0.432	32.8	0.665

It was considered that at least one-tenth inch would be required for returning the end of the winding to the terminal end, the crossing of wires for a calibration winding over the coil, and the placing of an electrostatic shield between the surface of the winding and the inside of the cover. Using this and available tubing sizes as criteria for selection of the cover tubing, and considering the values of H in Table 1 for only the odd numbers of layers, the number of layers chosen was 21.

Table 2 shows the tubing diameters and recapitulates other descriptive information.

Table 2

Cover Tubing I.D.	3.625 (in)
Coil Form O.D., r_1	2.250 (in)
Radial Space	0.688 (in)
Estimate of Coil Thickness, H	0.559 (in)
Remaining Space	0.129 (in)
Coil Length, 2C	40.4 (in)
Core Length, ℓ	72 (in)
Core Width, D	1.2 (in)
Estimate of Stacking Factor, s	0.90
Estimate of Core Area, A	1.30 $(in)^2$
Lamination Thickness, t	0.032 (in)
Number of Laminations	34

V. CONSTRUCTION

A. Materials and Core Construction.

Three different sizes of electrical grade, linen base, phenolic tubing were used in constructing the coils. Tubing used to enclose the core material and to serve as coil form had an outside diameter of two and one-fourth inches and a wall thickness of one-fourth inch. Three sections of this tubing were required to produce the overall length of $74\frac{1}{4}$ inches. Fitting over the coil form was tubing with an outside diameter of three and five-eighths inches and a wall thickness of eleven-sixteenths of an inch which was cut into rings. Used as a cover was tubing having an outside diameter of four and one-eighth inches with one-fourth inch wall thickness. Two sections of this tubing were fitted together for an overall length of $55\frac{3}{4}$ inches.

The core material consisted of strips of Allegheny Ludlum Mumetal 72 inches long, 1.2 inches wide, and 0.032 inch thick. Although an estimated stacking factor of 0.90 indicated that 34 strips could be placed in the coil form, it was found that the stacking factor was actually 0.95, permitting 36 strips in the allowable stack height of 1.2 inches. In the first two cores 36 strips were placed, but because of warping of the strips, only 34 could be placed in the third core.

Before placing the strips in the coil form, each strip was painted on both sides with Eccoseal W19 epoxy resin mixed with a 48-hour catalyst. The strips were stacked as they were painted. After pressing out the excess resin from the stack of strips, the coil form, sealed at one end with a

one-inch thick phenolic plug, was slipped over the stack and set upright on the closed end. A filler material and additional resin was then poured into the remaining space in the coil form until there was only sufficient space for another one-inch thick phenolic plug. This plug had a very shallow groove cut in it to allow for the escape of excess resin as it was seated in the coil form.

B. Retaining Rings, Closure Rings, and Separators.

Two rings of the above mentioned material, three-fourths inch wide, were used as retaining rings on each end of the allotted winding space. Two similar rings were used to close the cover tubing, the terminals being fitted into one of these.

From this same material were cut three spacers for separating the coil into four sections. These were fixed to the coil form with epoxy resin. For the first coil they were made one-eighth inch thick with a flange protruding an additional one-eighth inch on one side at the small diameter. The purpose of the flange was to provide sufficient contact area with the coil form to prevent end pressure of one section of the coil from breaking the separator loose from the form before the adjacent section could be wound. On winding the first section of the first coil, the flange caused difficulty in producing a neat winding, so the two remaining flanges were cut from their separators. For the second and third coils the separators were made three-sixteenths inch thick.

C. Coil Winding

Winding of the coils was accomplished on a lathe with a special bed extension that provided a bearing support just outside the retaining ring

farthest from the chuck. Another bearing support was fixed to the lathe bed near the chuck end of the coil. These bearings can be seen on the left and right, respectively, of Fig. 18 which shows a coil with the first section completed. In the rear can be seen the spool of wire which was turned by hand so that snags could be quickly spotted to prevent wire breakage. The wire was started against the coil form by slipping the end through a notch under the retaining ring. While being wound the wire was held tightly and wiped clean with a chamois skin. To the left of the center separator can be seen a clamp which was used to protect the separator from breakage while winding. After completion of a section, the clamp was carefully removed and fastened against the next separator. At the end of a section the wire was brought into the next section through a notch in the separator. When the last section was finished, the wire was brought out of the retaining ring through a small hole and back through a second hole, then along the coil through notches in the separators and out of the retaining ring at the start of the coil through a small hole diametrically opposite the starting end. Rather than impregnate the completed coil, each layer of wire was painted with epoxy resin before the next layer was wound. No other material was used between layers. Most of the winding was done at a speed of 132 rpm, the next lower speed, 86 rpm, being used occasionally. The number of turns was recorded on a counter attached to the lathe.

After the sensor winding was completed, a calibration winding of thirty turns was placed on the coil form, half at each end of the sensor winding, outside the retaining rings.

D. Internal Shield, Terminals, and Cover.

The finish end of the sensor winding and the wires connecting the halves of the calibration winding were separated from the sensor winding by a strip of polyethylene sheet in each section of the coil. Larger strips were then used to separate brass screen wire shields wrapped around each section. The section shields had previously been joined electrically by one copper wire, soldered at each end. This connecting wire was fitted into notches in the separators. As the shields were wrapped around the coil, care was taken in location of the end of the polyethylene strip to prevent shorting of the ends of the shield. Connection to the shield was made by one wire passed through a hole in the retaining ring at the start of the coil and soldered to the edge of the shield adjacent to the retaining ring. The shield was fixed in place with glass tape as shown in Fig. 19.

The closure rings and terminals are also shown in Fig. 19 where the sensor, calibration, and shield wires have been connected to the terminals and taped in place with glass tape. The terminals used on the sensor winding were made from electrolytic grade copper. They were washed in acetone and air dried before connecting the sensor winding. The ends of the sensor winding were rubbed with sandpaper to remove the Nyclad, wiped with a clean dry cloth, and fastened to the terminals with copper nuts. No special precautions were taken with the wires from the calibration winding and the shield; they were soldered to five-way binding posts. The spaces on the ends of the coil were filled with loosely wrapped glass cloth.

Before putting the cover on the coil, six holes were drilled in it so that each section of the coil and the two end sections could be filled with epoxy resin. The cover was then put on the coil and the ends sealed to the closure rings with resin. Fig. 19 shows a coil with the cover in place. Filling the cover with resin completed the assembly.

E. Boxes.

For reduction of capacitive pickup, protection of the sensors, particularly the terminals, from contamination by the weather, and for protection from accidental damage in handling, a box was constructed for each sensor from three-fourths inch marine plywood fastened together with brass screws and waterproof glue. Along the sides of the box and on the lid brass screen wire was used for electrostatic shielding. Faraday shields were used on the ends. These were made of 68 parallel pieces of B& S gauge 22 Nyclad wire, stripped on one end and soldered to a cross-wire. Spacing of the wires was insured by weaving four, one-fourth inch wide strips of wrapping paper through the array of wires. A sheet of glass cloth was sewn to each side of the shield before fixing it in the box with polyester resin and a rectangular piece of plywood. An excess of screen wire which extended above the top of the box about an inch was bent inward to allow clearance of the chest-type lid. The tops of the Faraday shields on the ends were also bent inward. After making a one-point solder connection between the Faraday shields and the screen wire, a strip of glass cloth was placed along the edge of the screen wire and painted with polyester resin to make a waterproof barrier around the top of the box.

The boxes were painted inside and ouside with several coats of polyester resin. All metal parts were either copper or brass.

Fig. 20 shows one of the boxes with the lid open and a sensor inside. The framework in the bottom of the box offers cradle support to the sensor cover tubing at five points. Over two of these are saddle pieces for holding the sensor in place. On the left is a split platform for supporting the sensor in a vertical position. On the right near the sensor terminals is an L-shaped brass terminal board which is soldered to the screen wire inside the box. Mounted on the horizontal part are two, five-way binding posts; the one on the right soldered in place, the other insulated. To the vertical side of the terminal board is fastened a brass tube with an inside diameter of one-half inch. It protrudes through the rear of the box about three-fourths inch. The cable is brought through this tube, its shield fastened to the right-hand five-way binding post, and its inner conductors fastened to the sensor terminals. As the lid is closed,a banana plug connected to the lid shield through a flexible copper strap is plugged into the right-hand five-way binding post.

VI. RESULTS OF THE WINDING OPERATION AND TESTING

A. Spacing Factors and Wire Length.

Table 3 shows the total number of turns placed on each coil, from which was calculated an average number of turns per layer. Using the bare wire diameter, the average length of copper per layer was then calculated. The ratio of the effective layer length, which does not include the spacers, to the copper length gives the axial spacing factor, K_2. By a similar procedure, the radial spacing factor was found to be the same as estimated. The length of wire listed in Table 3 was calculated from the measured wire resistance. Using the spacing factors in Table 3, the wire length given by Eq. (6) is 21.9 (kft) for coil No. 1 and 22.8 for coil Nos. 2 and 3. These figures are about two per cent greater than the resistance measurement indicates they should be.

B. Inductance and Some Related Approximations.

Two methods were used to measure the inductance of the sensors in circuits which were resonant at frequencies far below the self-resonant frequencies. The results were identical within the accuracy of the frequency measurement. Table 4 shows the values of inductance calculated from the measured frequency and capacity. Fig. 21 shows the first method used. The second method, shown in Fig. 22, was used to obtain the responses plotted in Fig. 23 in addition to the resonant frequencies.

If losses in the capacitor are neglected (bridge measurement of capacity showed no measurable dissipation), the bandwidth of the curves in

Table 3

	Sensor		
	1	2	3
Total number of turns	29,620	30,842	30,914
Average turns per layer	1,410.5	1.468.7	1,472.1
Effective layer length, (in)	40.4	40.4	40.4
Copper length along layer, (in)	35.7	37.2	37.2
Axial spacing factor, K_2	1.132	1.086	1.086
Radial spacing factor, K_1	1.05	1.05	1.05
Measured wire resistance, (ohms)	346.8	366.2	362.0
Calculated wire length, (kft)	21.49	22.69	22.43

Table 4

	Sensor		
	1	2	3
Resonant frequency, (cps)	9.0	8.7	8.8
Inductance, (henrys)	630	680	660

Fig. 23 should give an estimate of the maximum total losses in the sensors. For sensors 1 and 2 the equivalent total series resistance is

$$R_T = \frac{\omega L}{Q} = \frac{2\pi f L}{f/\Delta f} = 2\pi(\Delta f)\, L,$$

$$R_{T1} = 2\pi(0.2)(630) = 0.8 \text{ (k ohms)},$$

$$R_{T2} = 2\pi(0.3)(680) = 1.3 \text{ (k ohms)}.$$

If a nominal value of R_T is taken to be 1000 (ohms), about 750 (ohms) comprise the loss resistance in excess of wire resistance. As a first order approximation to the eddy current loss resistance, R_e of Fig. 1, the equation given by Legg[22] for a coil wound on an annular core having uniform flux density is used:

$$R_e = \frac{0.0413\, t^2}{\rho}\, \mu_1 L f^2$$

where t = lamination thickness, (cm)

ρ = lamination resistivity, ($\mu\Omega$ - cm)

μ_1 = relative permeability, assumed constant throughout the cycle

L = inductance, (henrys)

f = frequency, (cps).

$$R_e = 3.2\, f^2 \text{ (ohms)}$$

for $t = 0.032$ (in)

$\rho = 56$ ($\mu\Omega$ - cm)

$\mu_1 = 10^3$

$L = 660$ (henrys).

Since the permeability decreases toward the ends of the core, use of the permeability at the center gives a value of R_e which is high. Using 8.8 (cps) as a typical frequency for this measurement,

$$R_e = 250 \text{ (ohms)}.$$

About 500 (ohms) remain to be accounted for by hysteresis in the core and proximity effect and eddy currents in the copper of the winding, skin effect having been neglected already (see Sec. IIA). If the effect on these losses of frequency alone is considered, eddy current losses in the core become negligible compared to the wire resistance at one cycle per second. The remaining losses, of which the hysteresis and copper eddy current losses are proportional to the first and second powers of frequency, respectively, would probably be much less than wire resistance. Further testing could, of course, confirm these suppositions and provide information concerning the residual losses.

A formula given by Terman[23] for calculating the inductance of an iron-cored coil with an air gap is

$$L = \frac{3.19\, N^2\, (10)^{-8}}{\left(\frac{\ell}{\mu_1 A} + \frac{\ell_a}{A_a}\right)} \quad \text{(henry)},$$

where ℓ_a = length of air gap, (in)

A_a = area of air gap, $(\text{in})^2$

ℓ = length of core, (in)

A = area of core, $(\text{in})^2$.

For the approximation

$$\frac{\ell a}{A_a} << \frac{\ell}{\mu_1 A}$$

the equation for L becomes

$$L = \frac{3.19\,\mu_1 AN^2 (10)^{-8}}{\ell} \text{ (henry).}$$

Evaluation of this equation gives

$$L = 550 \text{(henrys)}$$

for $\mu_1 = 10^3$

$A = 1.38\ (\text{in})^2$

$N = 3(10)^3$

$\ell = 72$ (in).

Adjusting the constant term to that shown in the following equation gives the measured value of inductance for sensor number 2.

$$L = \frac{3.73\,\mu_1 AN^2 (10)^{-8}}{\ell} \text{ (henry).} \qquad (15)$$

C. Self-Resonant Frequencies and Distributed Capacity.

Because of extremely high terminal impedance at the major self-resonant frequencies, the curves of Fig. 24 were plotted so that the resonant frequencies could be obtained by extrapolating the slopes outside the resonant region to their points of intersection. Table 5 shows these results. The diagram in Fig. 25 shows the method of obtaining the data. The circuit is essentially the same as that of Fig. 22, except for the capacitor external to the sensor.

Table 5

	Sensor		
	1	2	3
Major self-resonant frequencies (cps)	222	208	213

By substituting a capacitor decade box for the sensor at a frequency of 5.0 (kc/s) and by adjusting the capacity until the voltmeter read the same as it did with the sensor connected, the distributed capacity was determined to be about 900 (pf). For comparison with Sec. VIB above, these results imply inductance values of 570, 650, and 620 (henrys) for sensors 1, 2, and 3, respectively.

The distributed capacity of one section of a four-section coil can be calculated using the following formula which, except for notation and estimation of the distance between layers, is due to Terman:[24]

$$C_d = \frac{0.30\,\pi(r_1 + \frac{H}{2})\,C\epsilon_r}{(K_1 - 1)\,d\lambda} \quad \text{(pf)} \tag{16}$$

where

ϵ_r = average dielectric constant of insulation between layers.

The capacity per section becomes

$$C_d = 3,320 \text{ (pf)}$$

for $r_1 = 1.125$ (in)

$H = 0.558$ (in)

$C = 20.2$ (in)

$\epsilon_r = 3.3$

$$K_1 = 1.05$$

$$d = 0.0253 \text{ (in)}$$

$$\lambda = 21.$$

For the entire sensor, the capacity may be assumed to be one-fourth of this value or 830 (pf).

D. Rotation About Mid-Point.

As an alternative to calibrating the sensors in a time varying magnetic field, they could be spun about their mid-points in a constant field. Such a field is readily available as the constant component of the earth's magnetic field. If the above theories are correct, the sensitivity determined in this manner should be a few per cent higher than the sensitivity at the micropulsation level. Two problems exist in this method: rotation of the sensor at a constant, known angular velocity, and measurement of the component of the earth's field in the plane of rotation.

Using Eq. (14) the sensitivity equation can be derived by substituting for Z outside the parenthesis,

$$Z\left(1 - \frac{Z^2}{3}\right) = \frac{K_2 d\sqrt{F}}{\ell\lambda}\left(\frac{K'}{\mu_1}\right)$$

$$\frac{C}{K_2 d}\,\lambda\left(1 - \frac{Z^2}{3}\right) = \frac{K'}{\mu_1} \quad ,$$

and since $$N = \frac{2C}{K_2 d}\,\lambda,$$

$$K' = \mu_1 \frac{N}{2}\left(1 - \frac{Z^2}{3}\right)$$

or

$$E_p = \omega \mu_1 \mu_o H_o AN \left(1 - \frac{Z^2}{3}\right). \qquad (17)$$

Evaluation of Eq. (17) for the three sensors is shown in Table 6.

Table 6

	Sensor		
	1	2	3
Sensitivity, E_p, $\frac{(\mu v)}{(\text{gamma})(\text{cps})}$	150	156	149
Core area, A, $(\text{in})^2$	1.38	1.38	1.31
Total number of turns, N	29,620	30,842	30,914
Relative coil length, Z	0.532	0.532	0.532
Permeability at core mid-point, μ_1	1000	1000	1000

A simple experiment was performed as a rough check on the assumptions concerning the core permeability. Sensor number 3 was fastened to a small bearing plate on the floor of a steel reinforced building and spun by hand while the frequencies were determined by stop watch. The results are collected in Table 7. Calculated voltages are based on an ambient field of 27,000 gamma.

$$E_p = 149(27,000)\ \frac{(\mu v)}{(\text{cps})}$$

$$E_p = 4.0\ \frac{(\text{volts})}{(\text{cps})}$$

Table 7

Method	f	E_p (volts) Calc	E_p (volts) Meas
Strip chart	0.33	1.32	1.16
	0.34	1.36	1.16
Visually on VTVM	0.50	2.0	2.1
	0.83	3.3	3.5
	1.0	4.0	4.0

E. Miscellaneous.

The calibration winding impedance and its coefficient of coupling to the sensor winding was found at a frequency of 60 (cps). The sensor winding was connected to a variable transformer set at 100 (volts), for which the calibration winding produced a voltage of 70 (mv). Since the turns ratio was 10^3, the coefficient of coupling was 0.70. With the sensor winding being driven at 100 (volts), the calibration winding was shorted through a 0.1 (ohm) meter shunt, producing a short-circuit of 76.5 (ma). Dividing the open-circuit voltage by the short-circuit current gives an impedance of 0.915 (ohm). Subtracting vectorially, the 0.41 (ohm) d-c resistance leaves 0.818 (ohm) reactance, or an inductance of 2.17 (mh).

Weight of the sensors was 94 pounds each; the box weight 90 pounds.

There was no measurable d-c offset voltage at the sensor terminals.

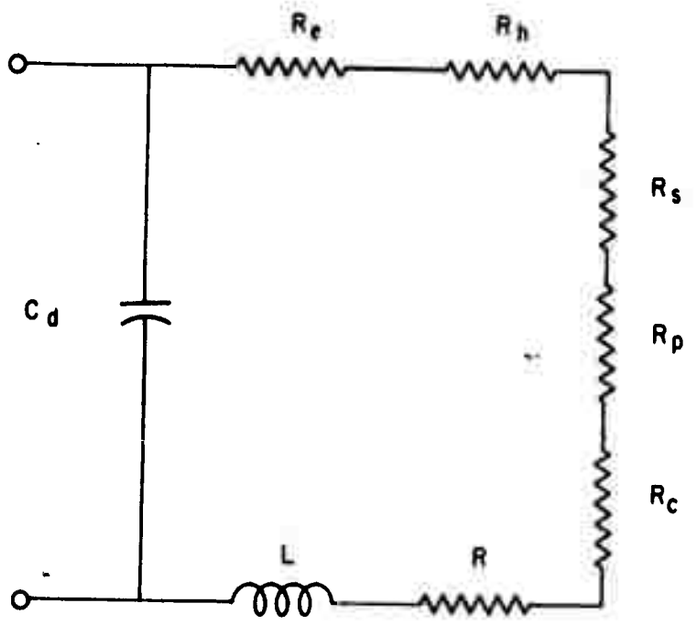

FIG. 1. EQUIVALENT CIRCUIT OF SENSOR WITH MAGNETIC CORE

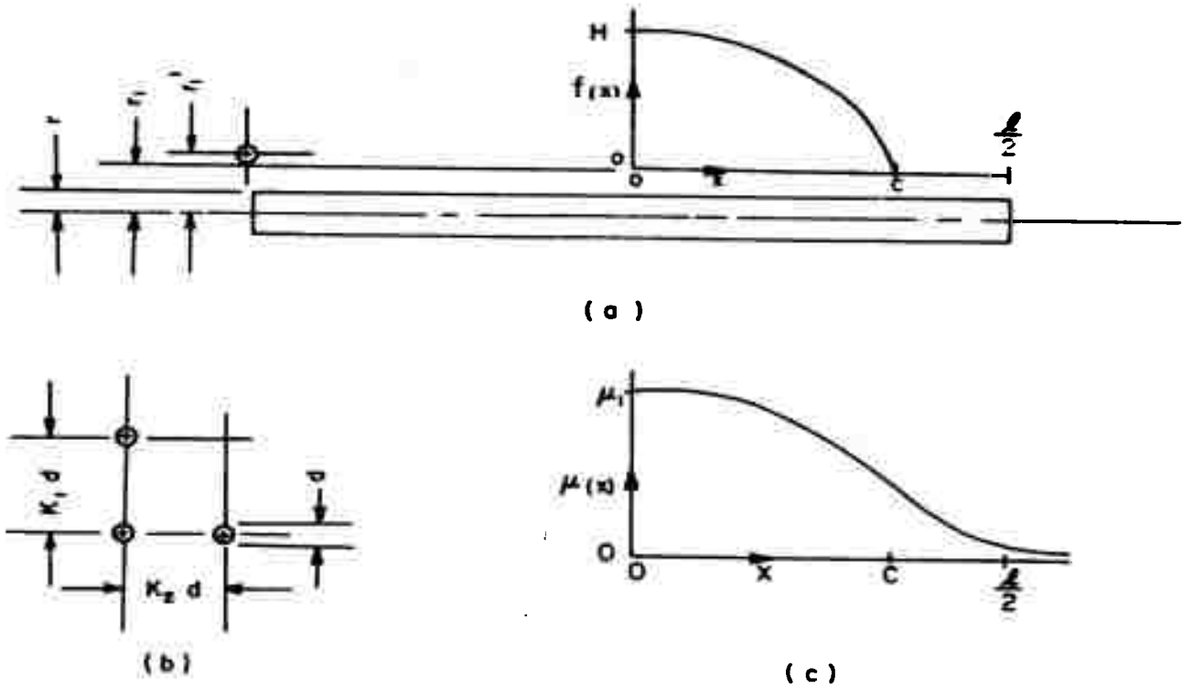

FIG. 2. DIAGRAMS SHOWING DIMENSIONS OF COIL AND PERMEABILITY FUNCTION. (a) LOCATION OF ENVELOPE OF COIL WITH RESPECT TO THE CORE. (b) METHOD OF MEASURING RADIAL WIRE SPACING FACTOR K_1 AND AXIAL WIRE SPACING FACTOR K_2. (c) METHOD OF SPECIFYING RELATIVE PERMEABILITY ALONG THE CORE.

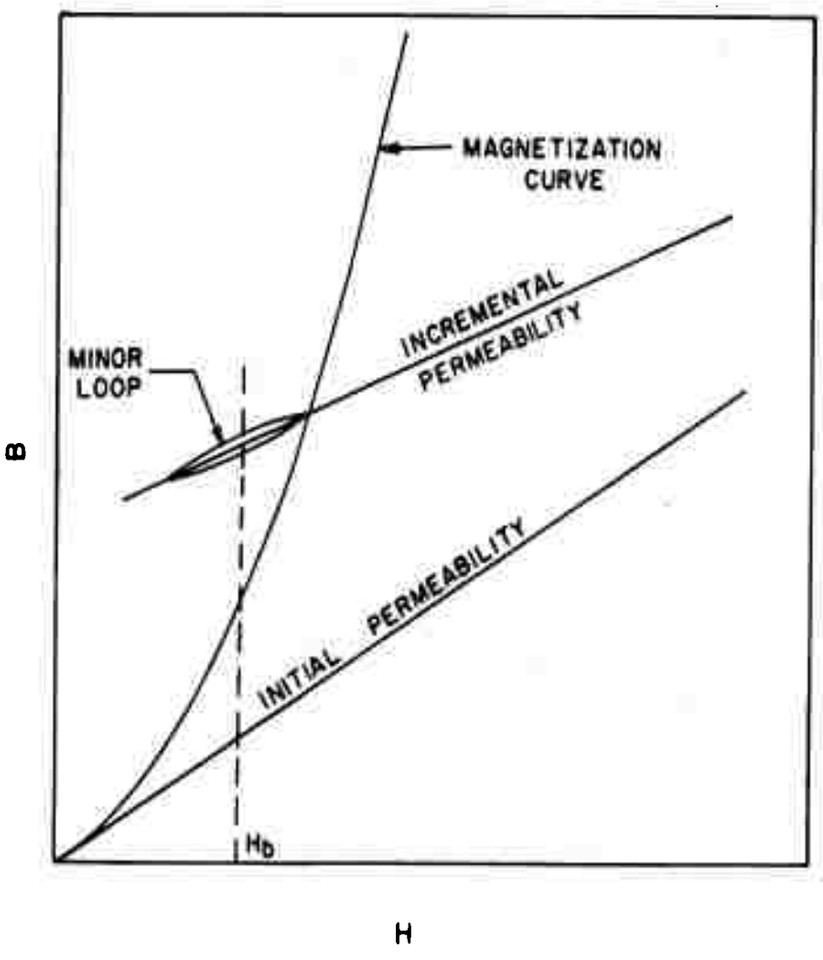

FIG. 3. MINOR HYSTERESIS LOOP CAUSED BY MICROPULSATIONS IN A CONSTANT FIELD H_b

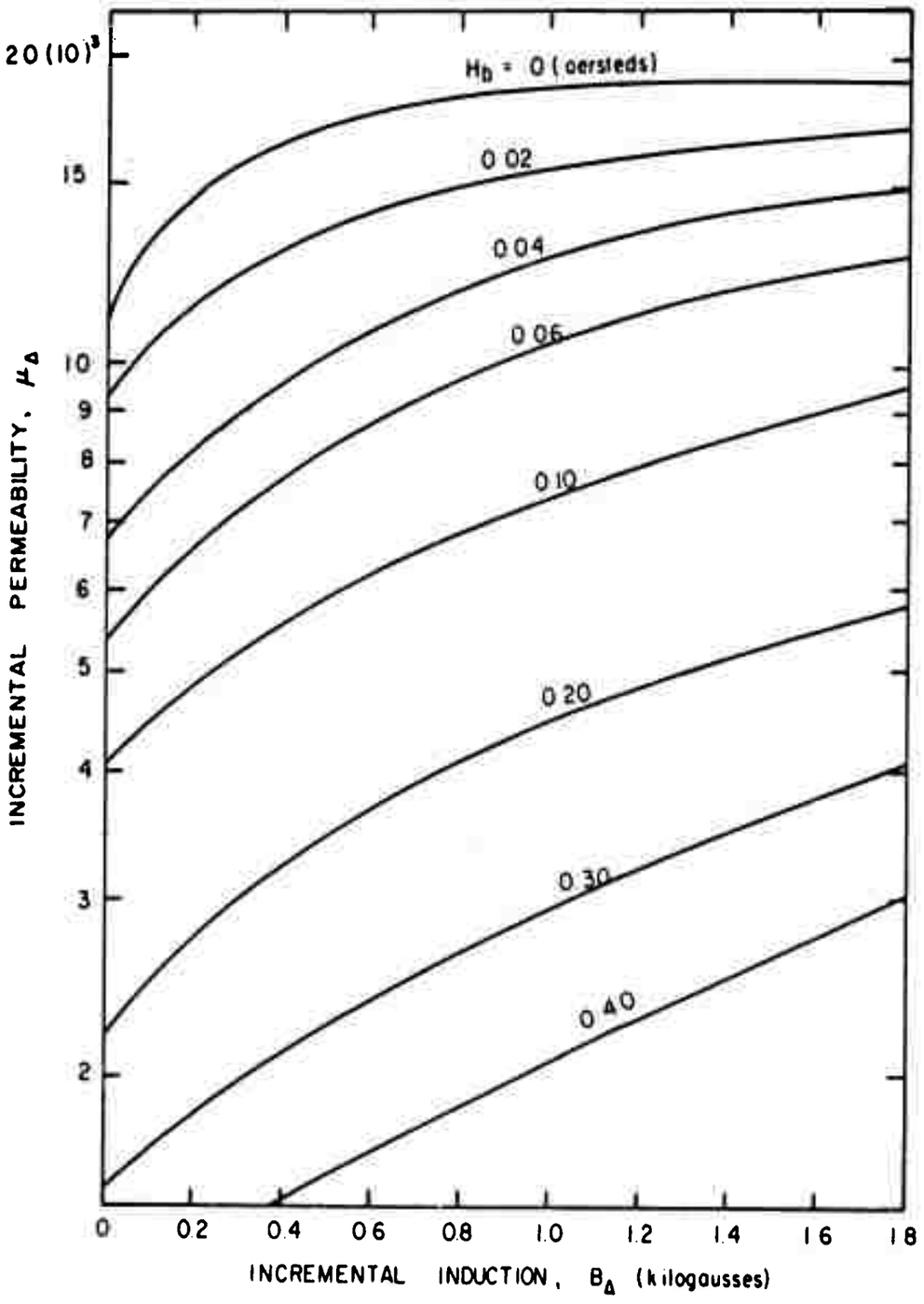

FIG. 4. 60 - CYCLE INCREMENTAL PERMEABILITY CHARACTERISTIC, 0.014" MUMETAL (E.I. LAMINATIONS 100% INTERLEAVED). REPRODUCED COURTESY ALLEGHENY LUDLUM STEEL CORPORATION

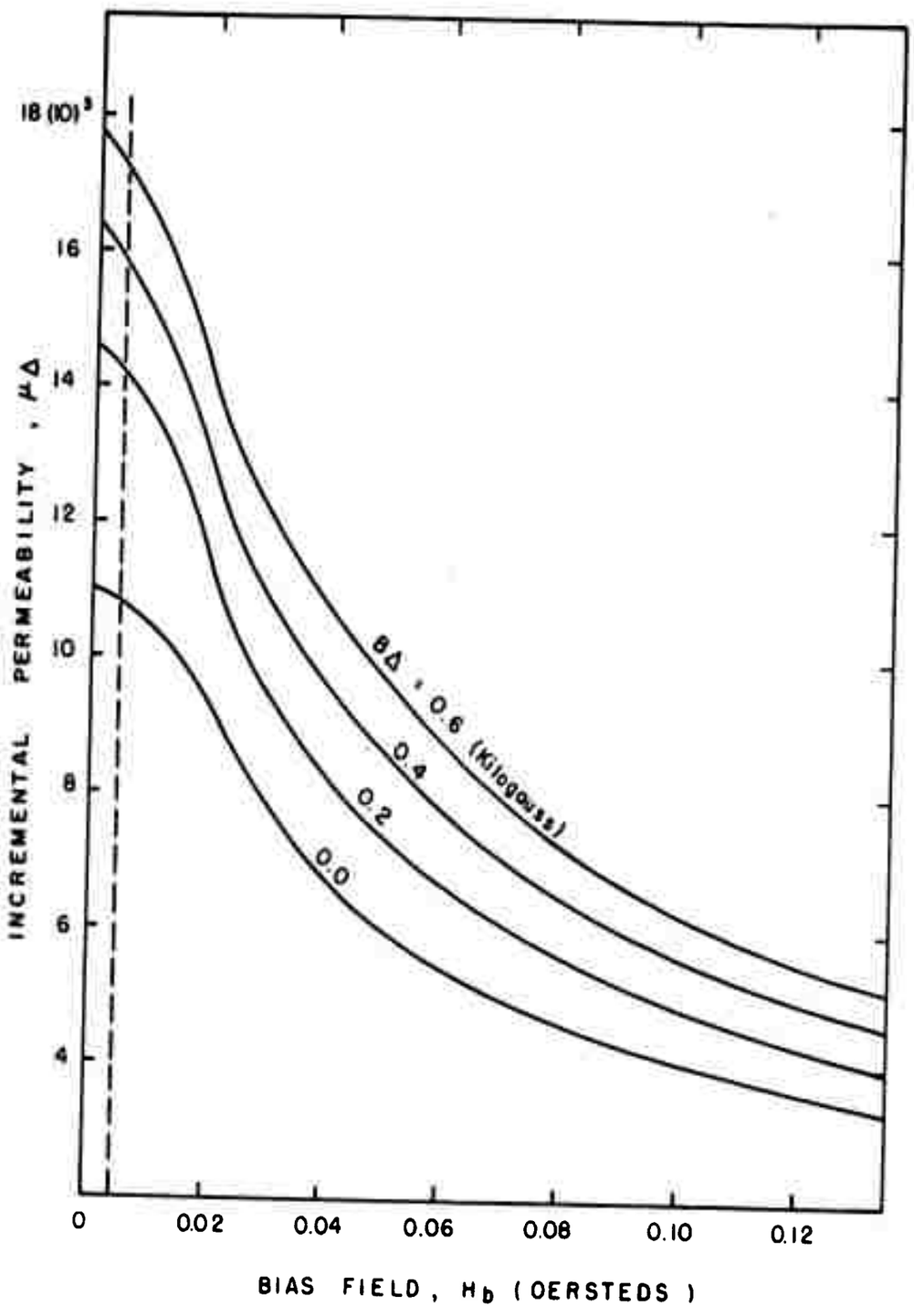

FIG. 5. INCREMENTAL PERMEABILITY AS A FUNCTION OF BIAS FIELD

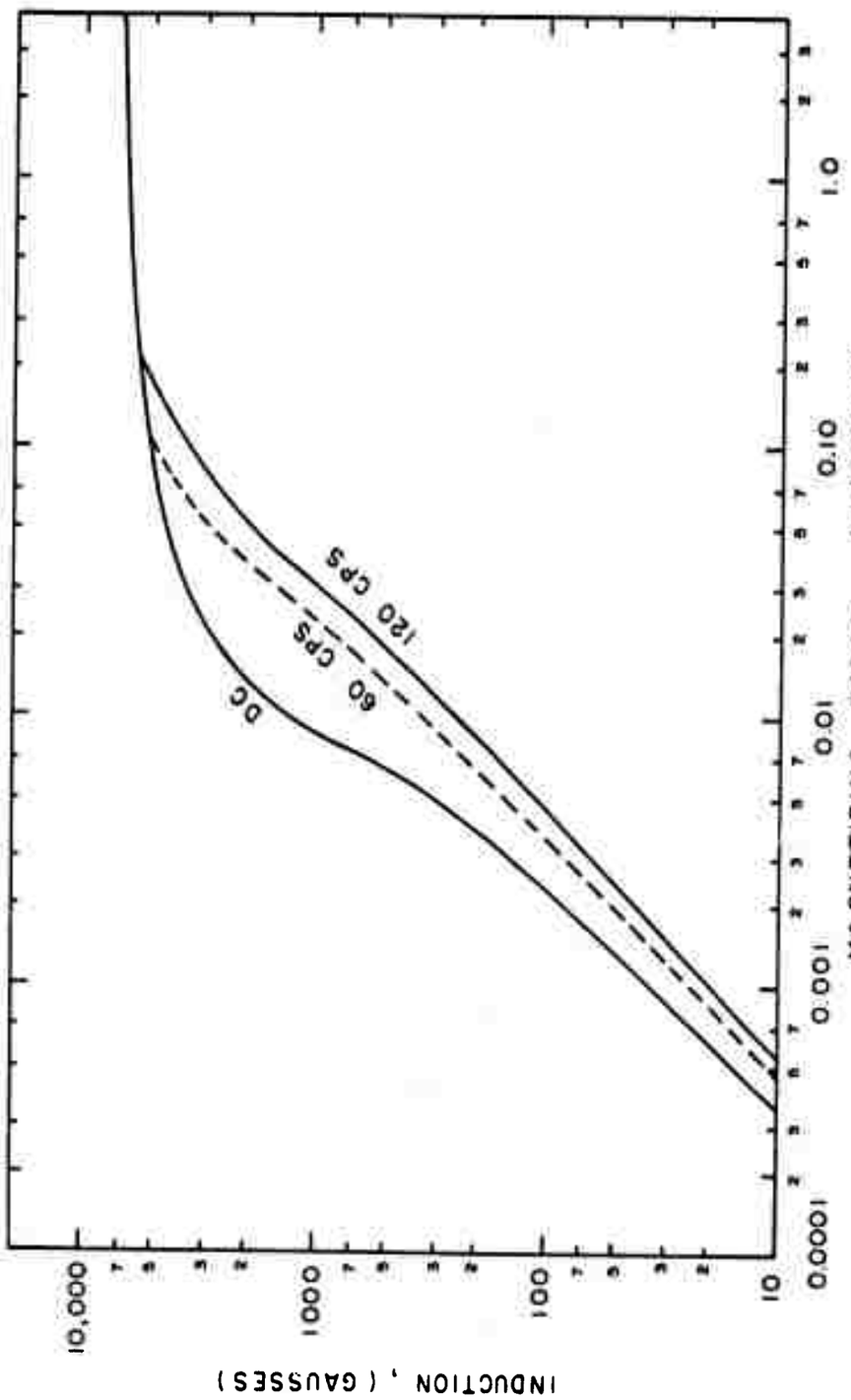

FIG. 6. MAGNETIZATION CURVES, 0.014" MUMETAL (STAMPED RINGS, 2.5 "OD, L9" ID, SAMPLE : 35175). REPRODUCED COURTESY ALLEGHENY LUDLUM STEEL CORPORATION

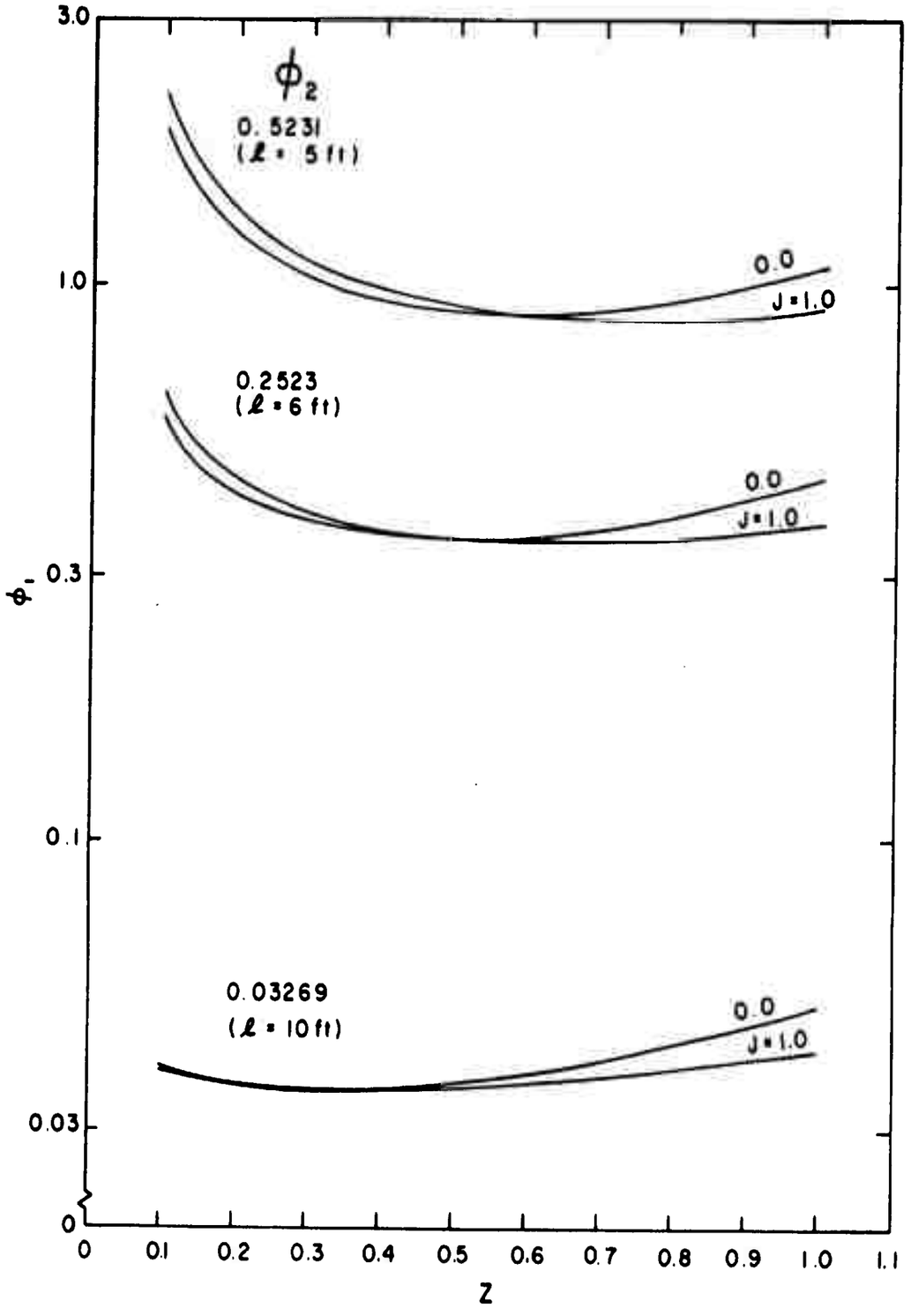

FIG. 7. ϕ_1 VERSUS Z SHOWING EFFECT OF ϕ_2

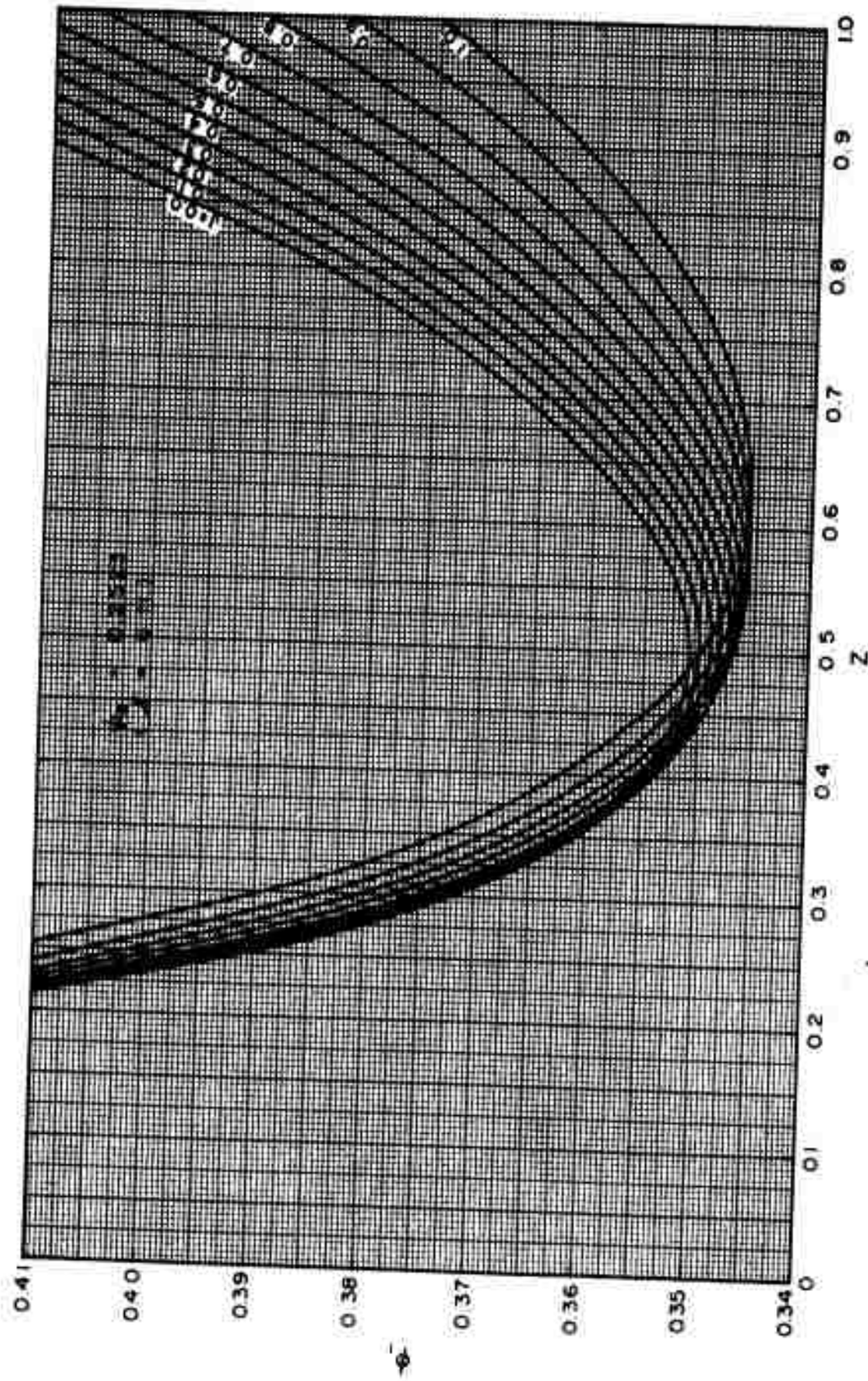

FIG. 8. ϕ_1 VERSUS Z SHOWING EFFECT OF J

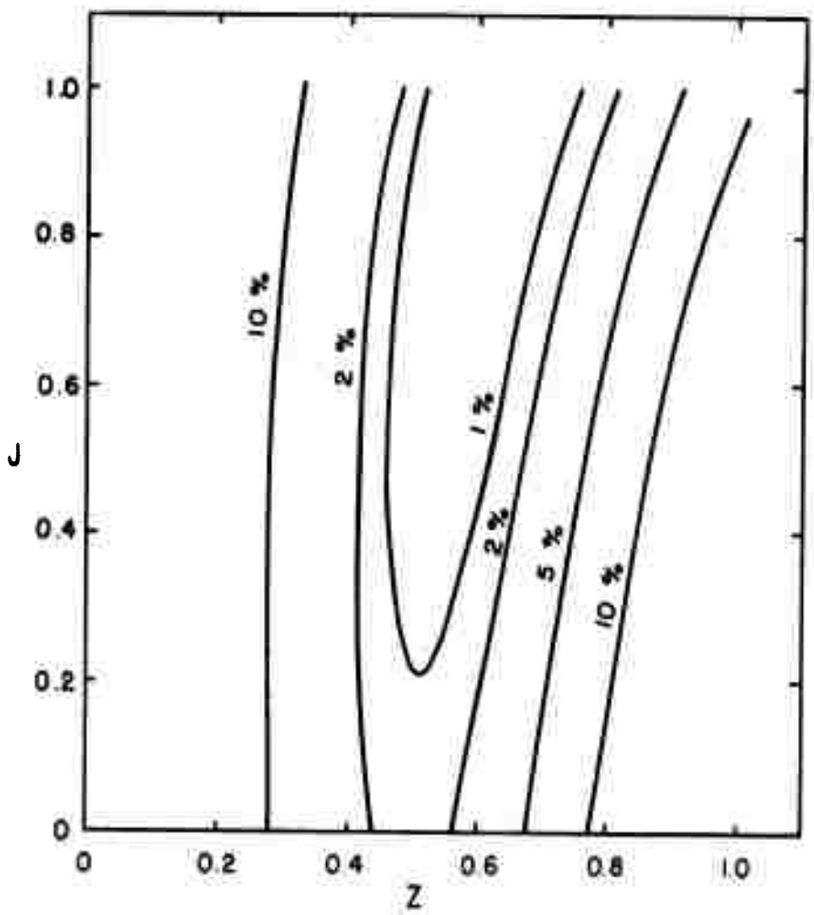

FIG. 9. CONTOURS OF CONSTANT ϕ_1, GREATER THAN THE MINIMUM FOR $\phi_2 = 0.2523$ ($\ell = 6$ FT.)

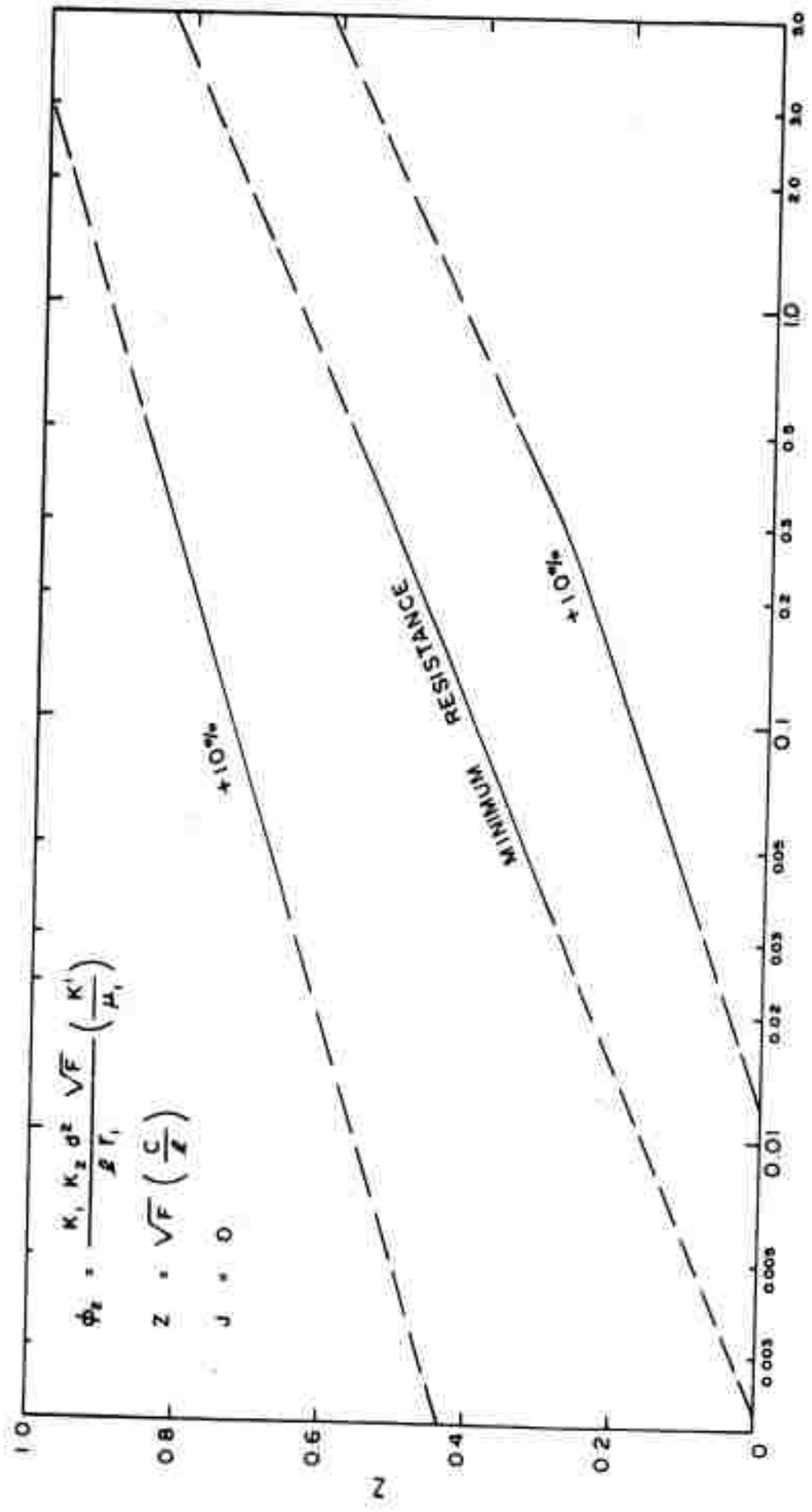

FIG. 10. RELATIVE COIL LENGTH AS A FUNCTION OF ϕ_2 FOR MINIMUM RESISTANCE IN A CYLINDRICAL COIL

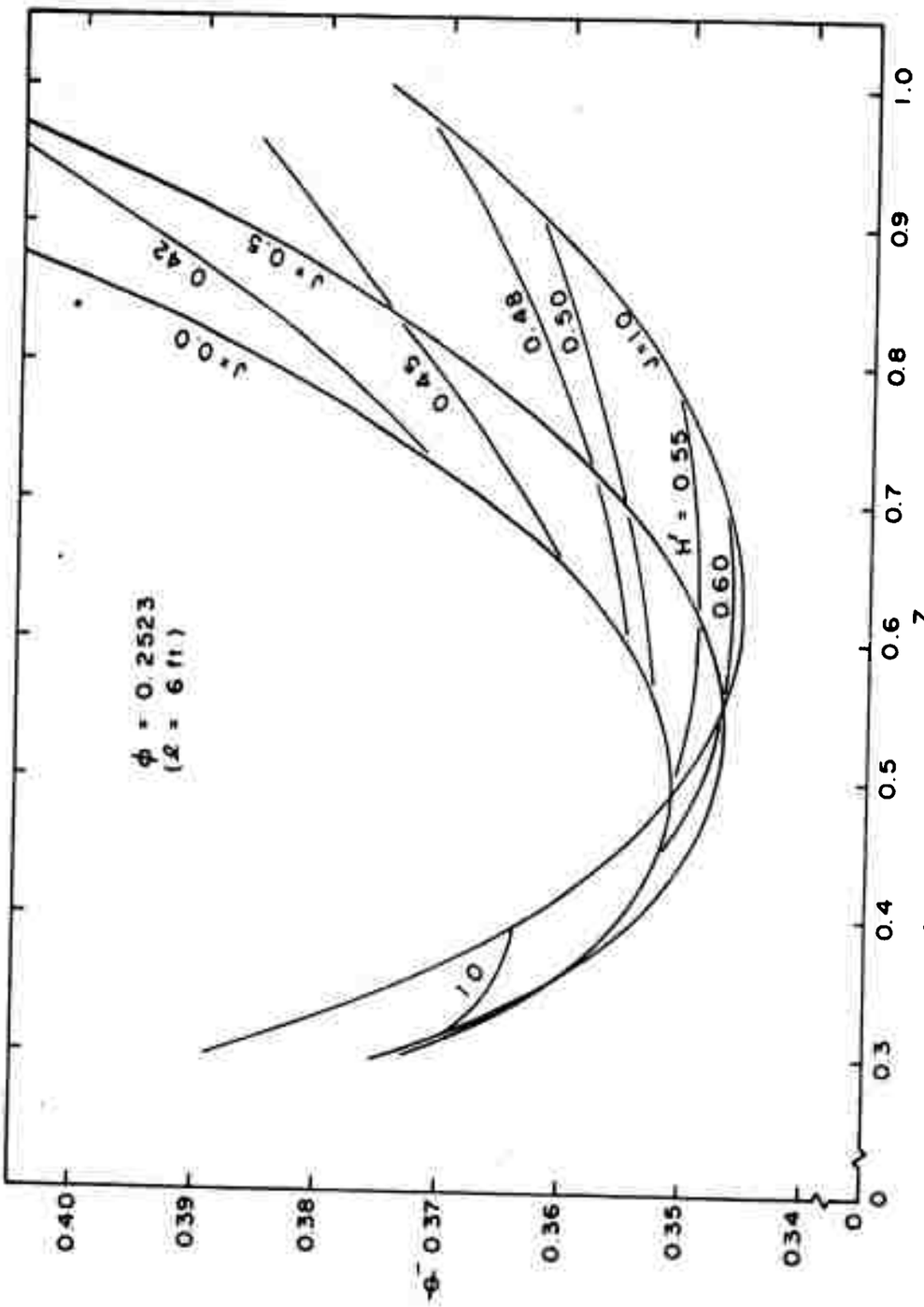

FIG. 11. ϕ_1 VERSUS Z SHOWING EFFECT OF H'

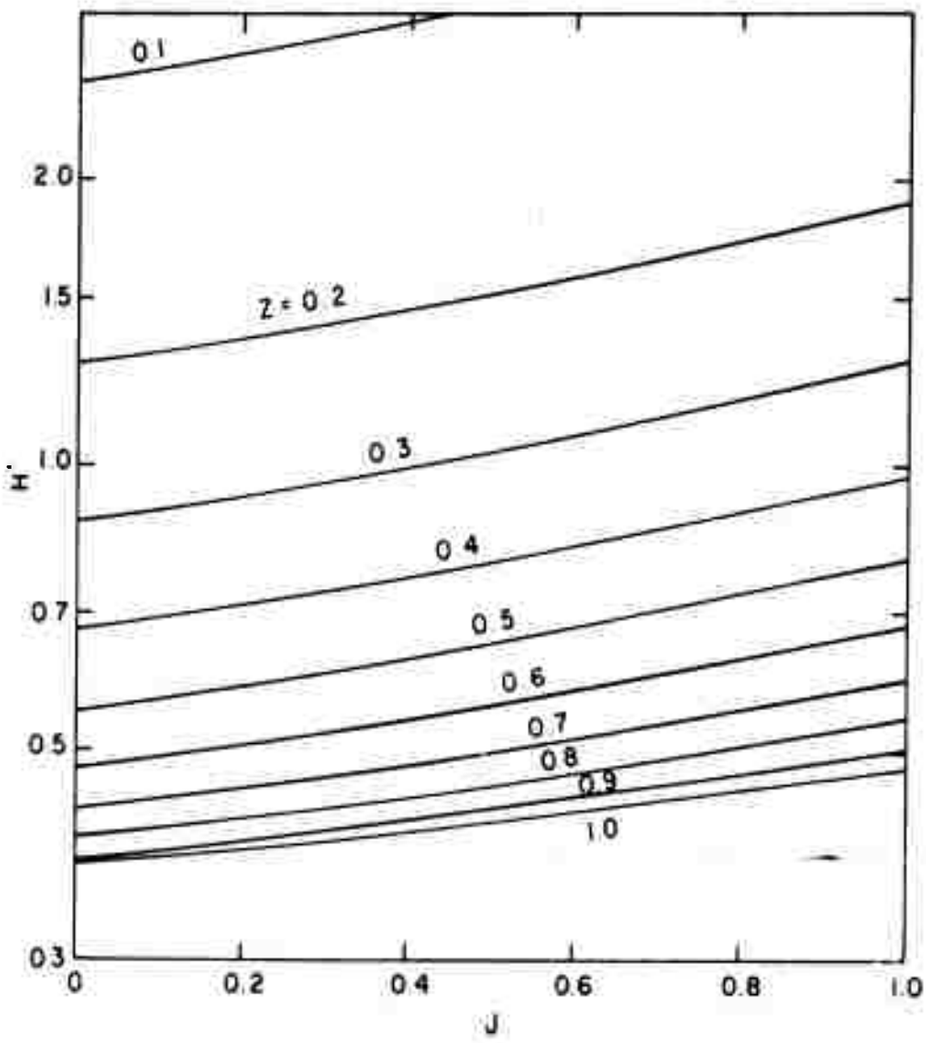

FIG. 12. RELATIVE COIL THICKNESS, H' VERSUS J

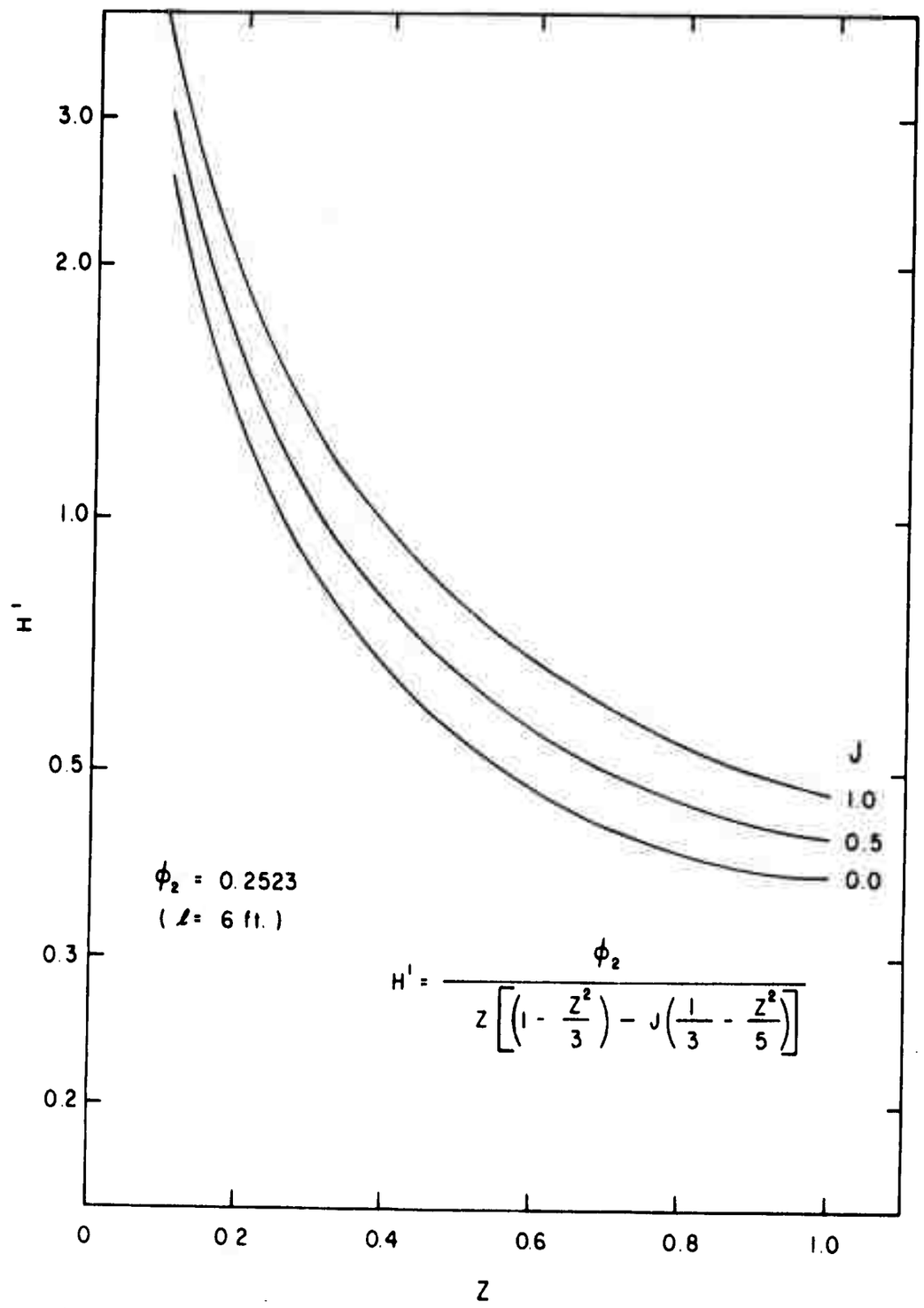

FIG. 13. RELATIVE COIL THICKNESS, H' VERSUS Z

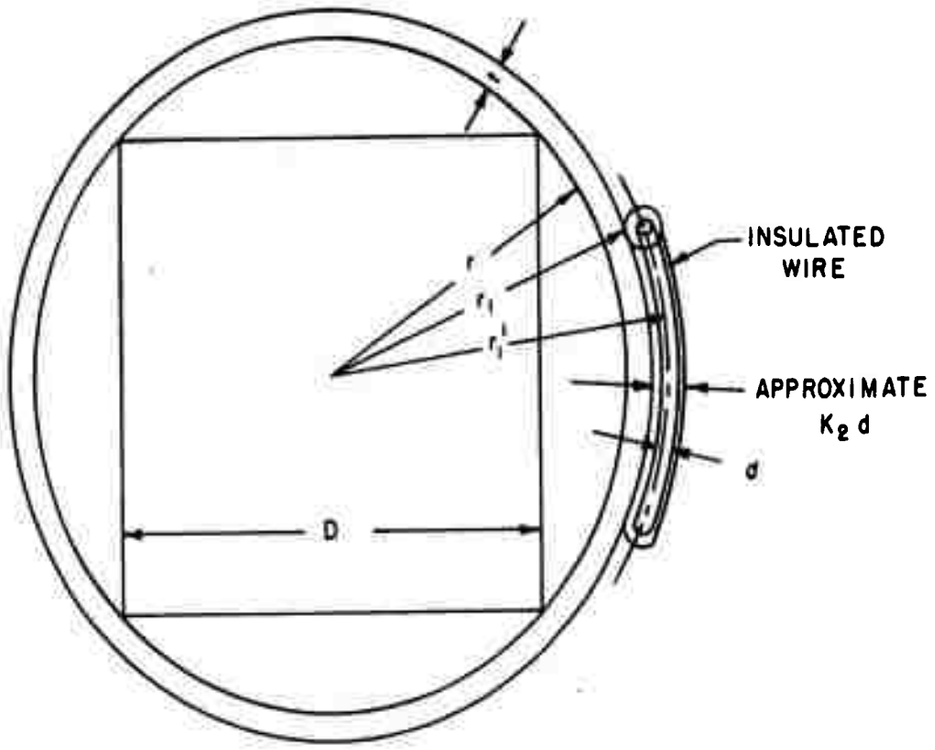

FIG. 14. END VIEW OF COIL FORM CONTAINING SQUARE CORE

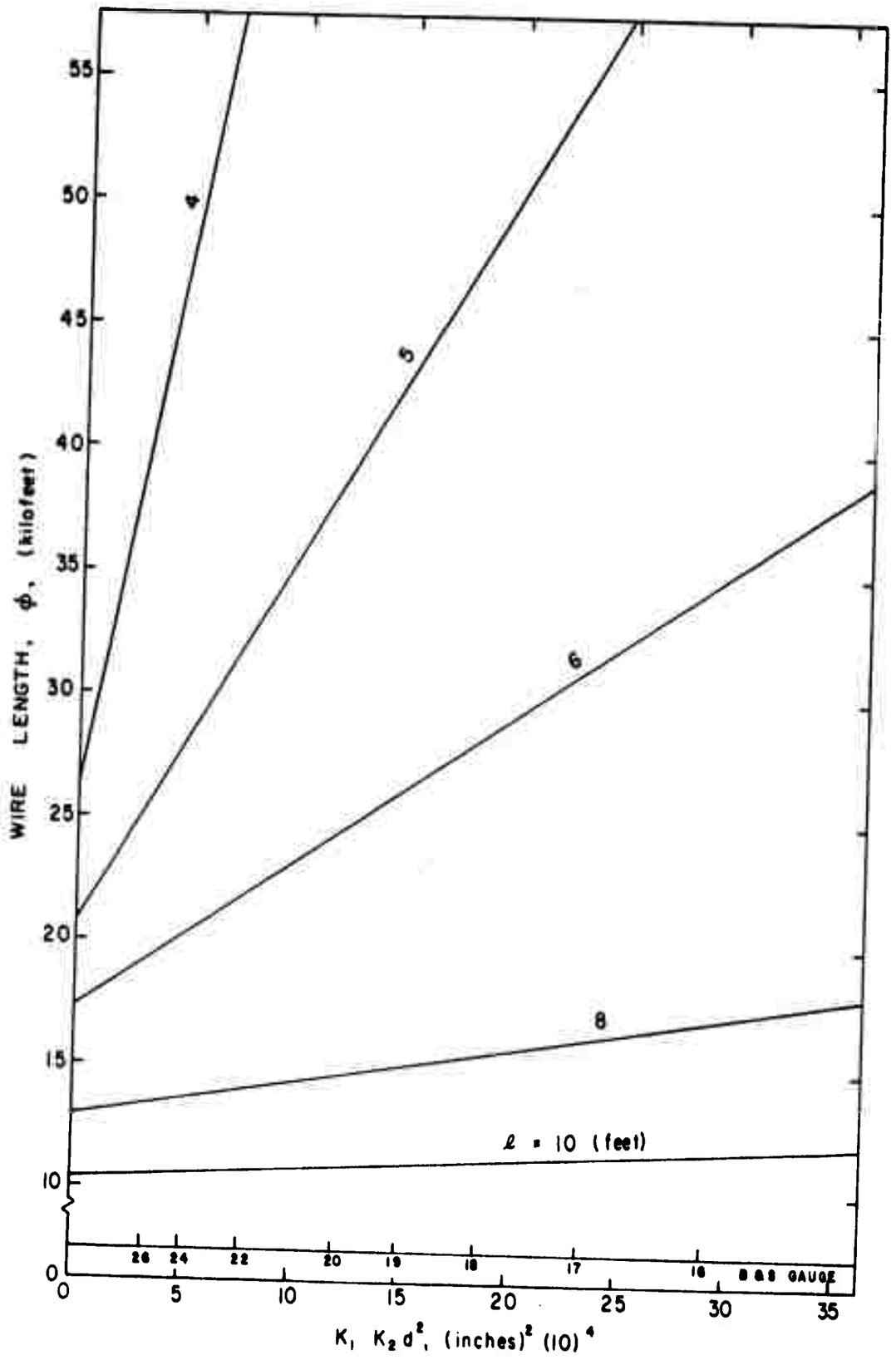

FIG. 15. WIRE LENGTH VERSUS WIRE DIAMETER SQUARED

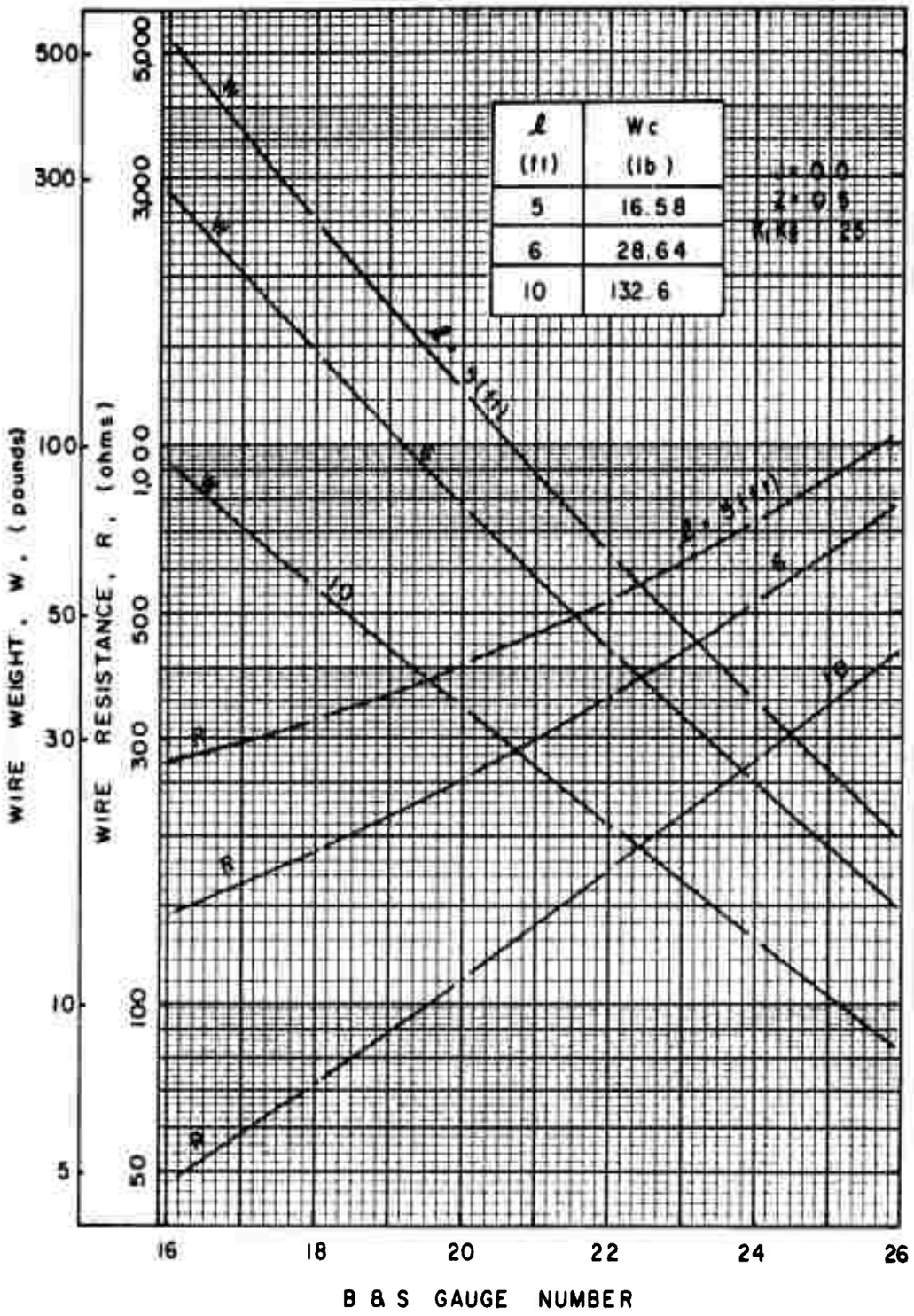

FIG. 16. WEIGHT AND RESISTANCE VERSUS GAUGE NUMBER

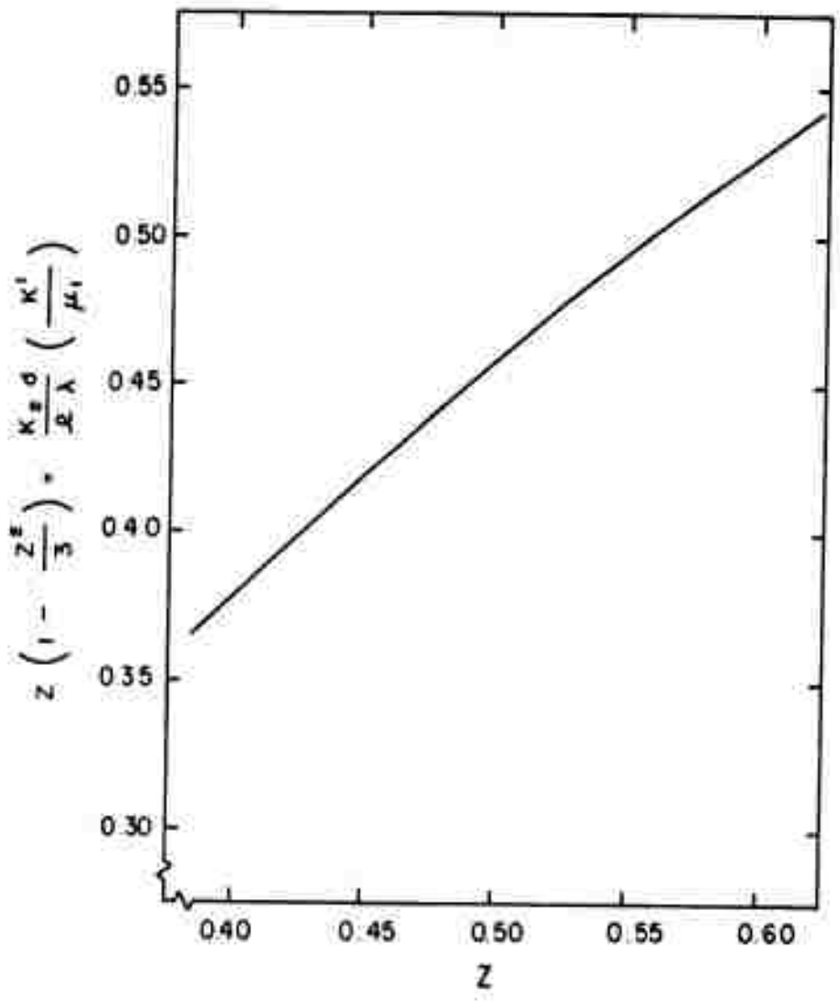

FIG. 17. SOLUTION OF EQUATION (14)

FIG. 18. PARTIALLY WOUND COIL

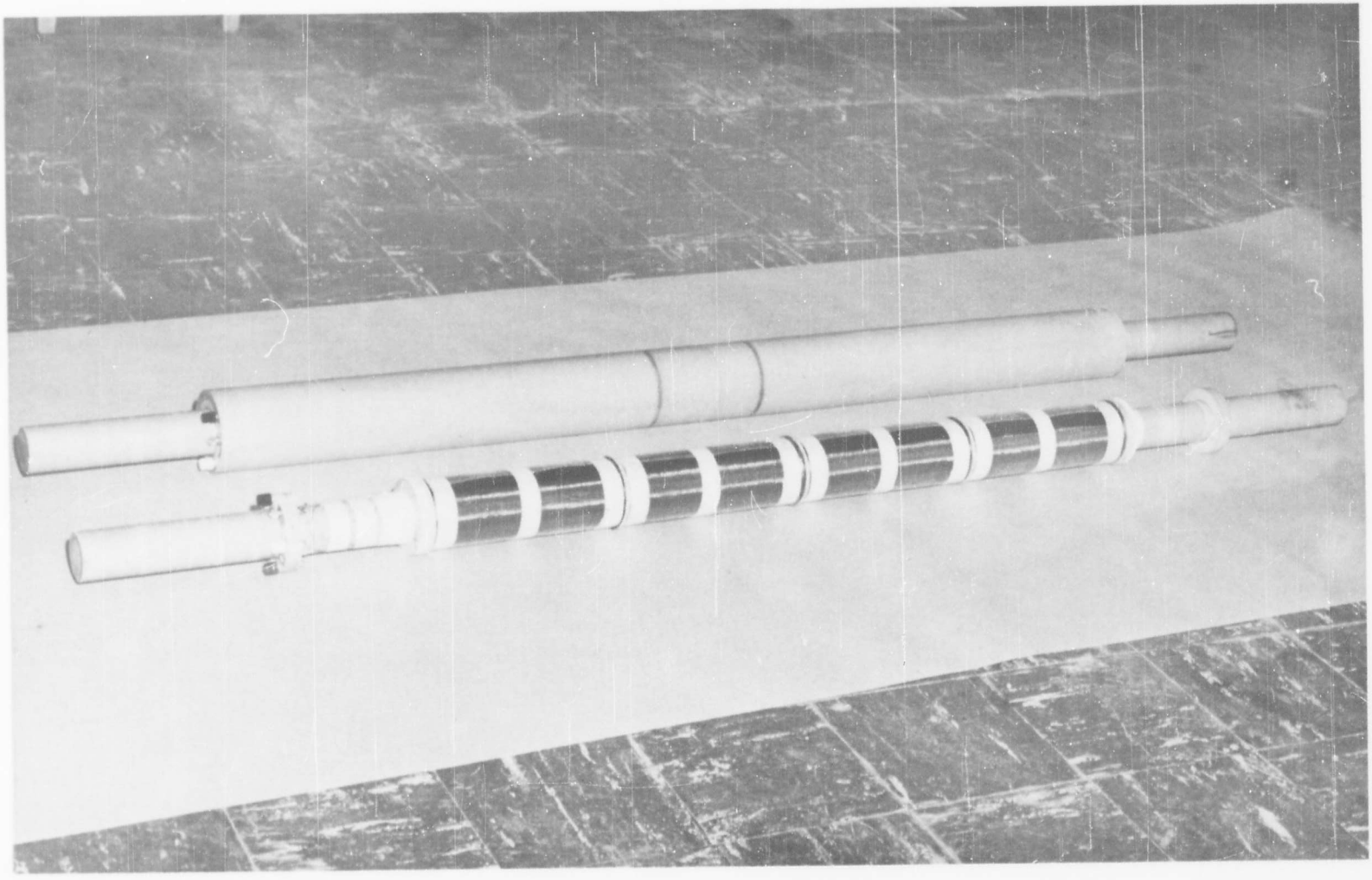

FIG. 19. SENSORS WITH AND WITHOUT COVER

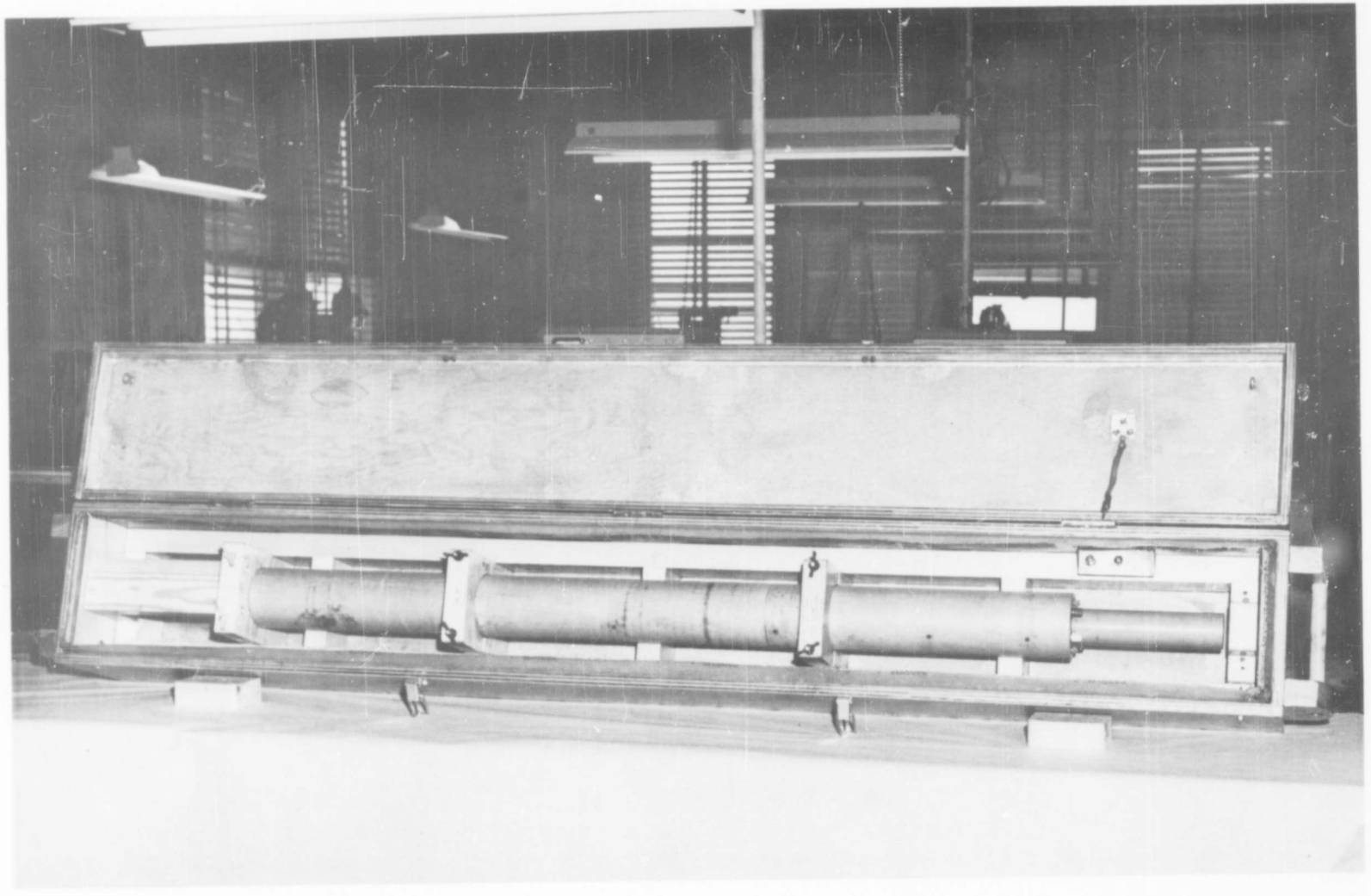

FIG. 20. COMPLETED SENSOR IN SHIELDED BOX

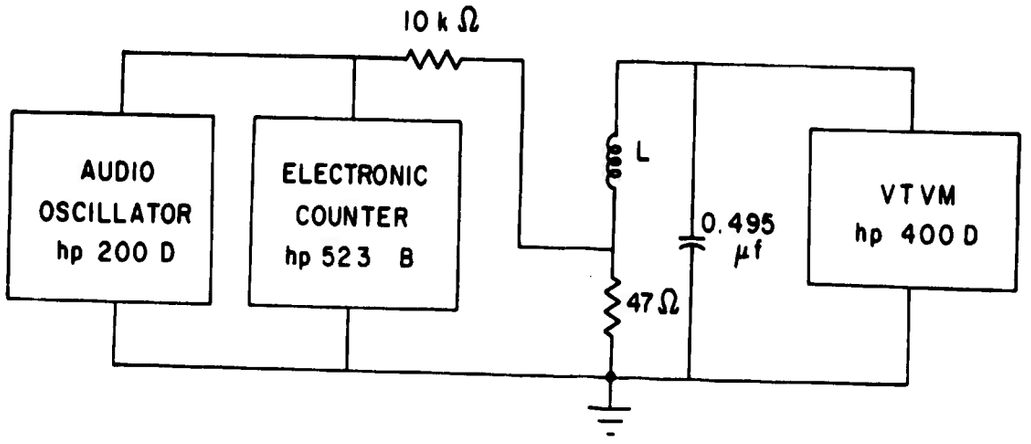

FIG. 21. FIRST METHOD OF MEASURING INDUCTANCE

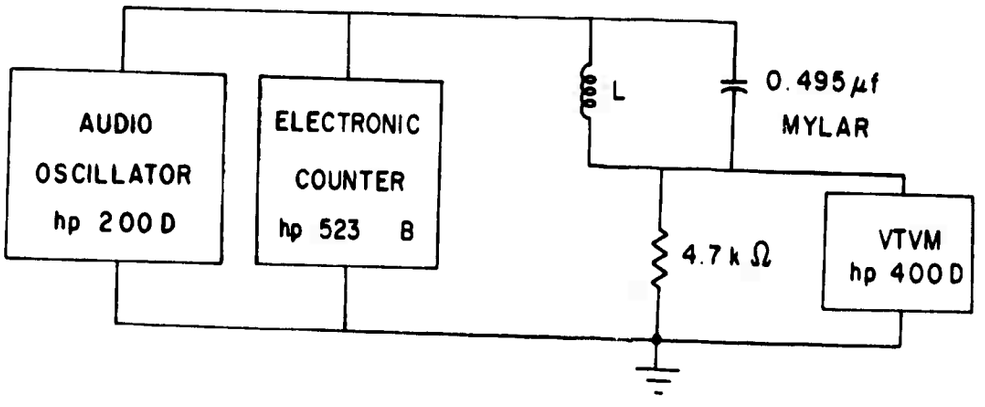

FIG. 22. SECOND METHOD OF MEASURING INDUCTANCE

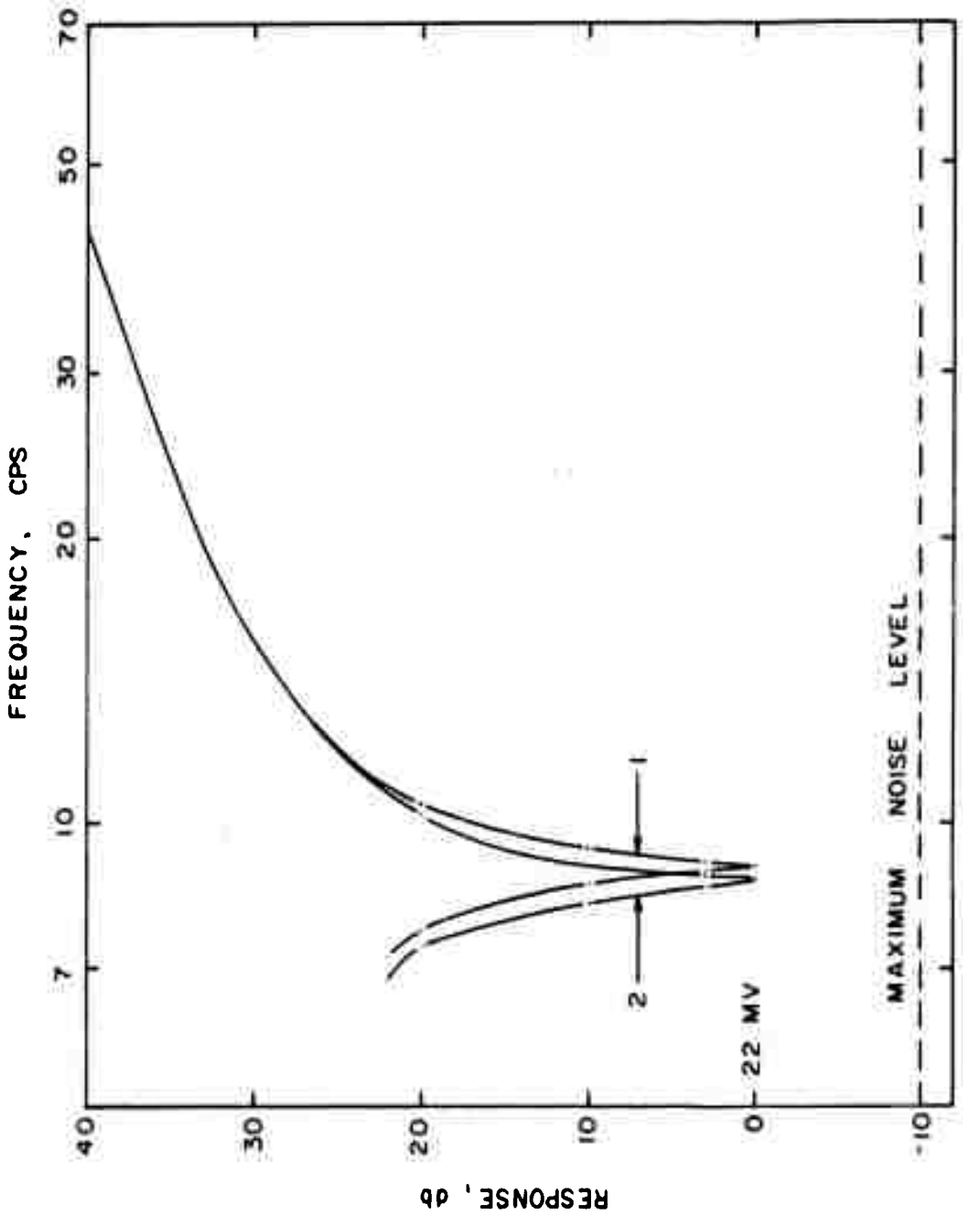

FIG. 23. RESPONSE USING CIRCUIT OF FIG. 22.

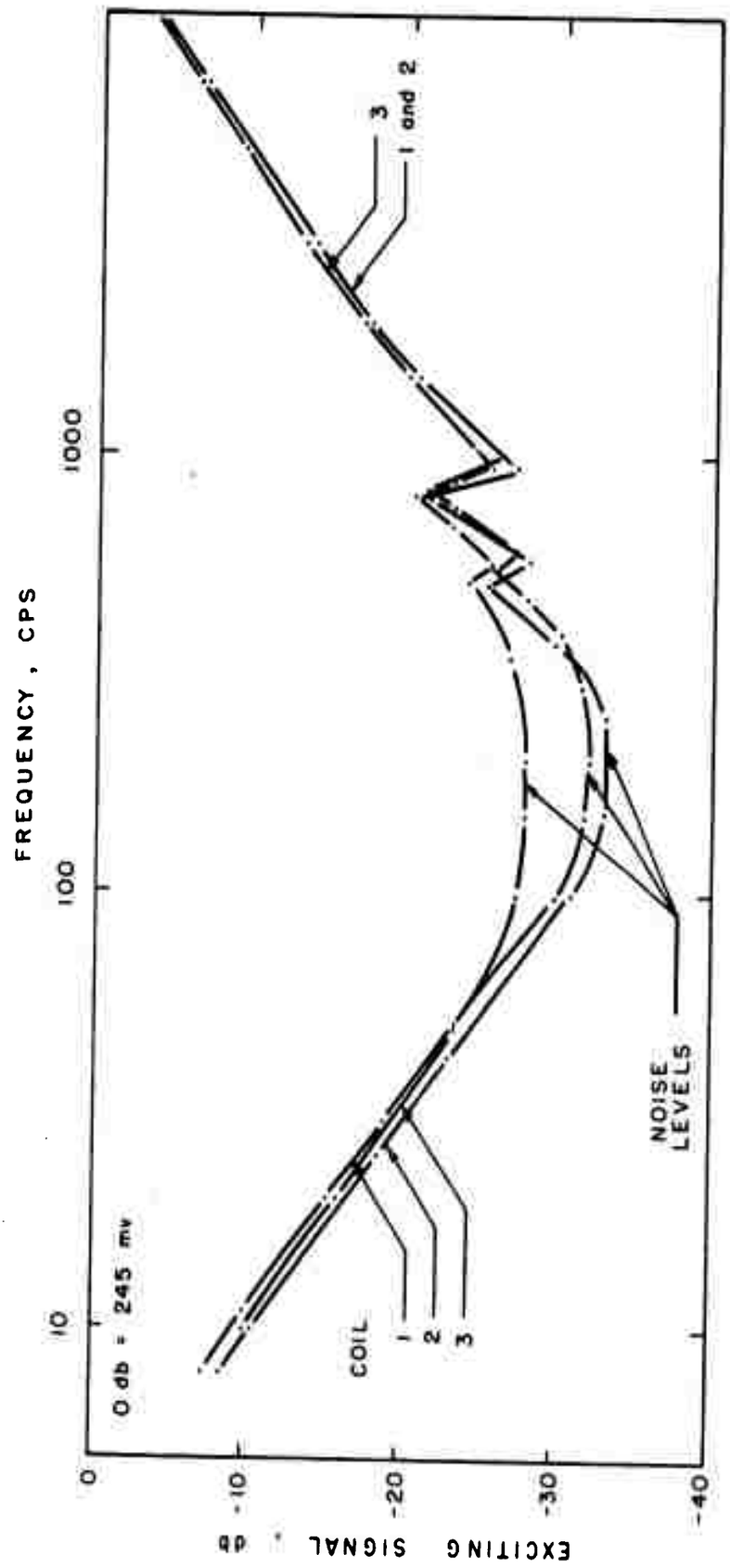

FIG. 24. SENSOR FREQUENCY RESPONSES

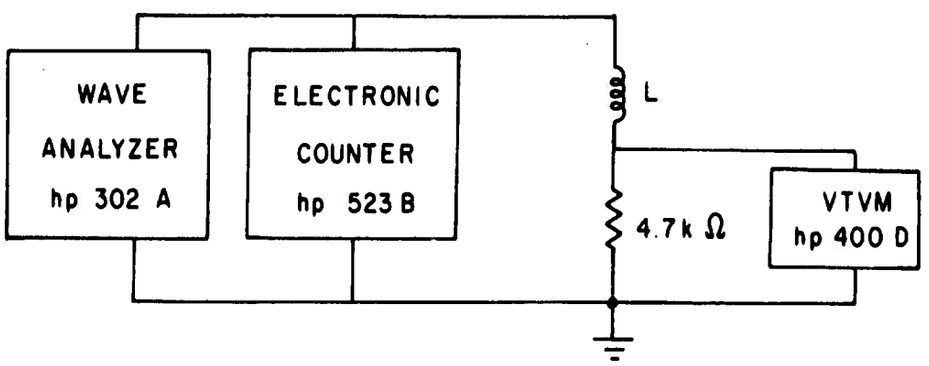

FIG. 25. CIRCUIT FOR DETERMINING SELF-RESONANT FREQUENCIES

LIST OF SYMBOLS

A	Cross-sectional area of core material
B	Magnetic flux density
C	One-half the length of the winding
C_d	Distributed capacity
D	Diameter of a cylindrical core; length of side of square core
d	Diameter of bare wire
E	Voltage induced in the winding, rms
E_p	Voltage induced in the winding, peak
e	Instantaneous induced voltage
F	Permeability shaping factor, dimensionless
f	Coil thickness as a function of distance from mid-point
h	Instantaneous ambient magnetic field intensity, neglecting static component
H_o	Peak value of alternating component of ambient magnetic field
H	Mid-point thickness of the winding
H'	Relative coil thickness, dimensionless, $\frac{H}{r_1}$
J	Coil shaping factor, dimensionless
K	Voltage proportionality constant, $\frac{\omega \mu_o H_o A}{\sqrt{2}}$
K'	Dimensionless sensitivity constant, $\frac{E}{\sqrt{2}\,\omega \mu_o H_o A}$
K_1	Radial spacing factor, dimensionless
K_2	Axial spacing factor, dimensionless
L	Inductance of winding due to core and air

ℓ	Length of core material
N	Total number of turns in winding
n	Number of turns in half of the first layer of the winding
Q	Quality factor
R	Direct current resistance of winding
R_c	Resistance representing eddy current losses in winding
R_e	Resistance representing eddy current losses in core
R_h	Resistance representing hysteresis losses in core
R_p	Resistance representing proximity effect in winding
R_s	Resistance representing skin effect in winding
R_T	Total effective resistance in series with winding
r	Radius of cross-sectional area containing core material
r_l	Coil form radius
r_l'	Mean radius of smallest turn of wire
s	Stacking factor of laminated core
T	Number of turns stacked radially
t	Coil form thickness; lamination thickness
W	Wire weight
W_c	Core weight
x	Axial distance from mid-point of core
Z	Relative coil length, dimensionless, $\sqrt{F}\,\frac{C}{I}$
λ	Number of layers of wire in the center of the coil
μ_o	Permeability of free space

μ_1 Effective relative permeability at mid-point of core

μ Effective relative permeability as a function of distance from mid-point of core

ϕ Total length of wire in winding

ϕ_A Length of wire required to connect turns and to connect layers

ω Radian frequency

ϵ_r Average dielectric constant

APPENDIX A

Derivation of the General Formulae

Consider a cylindrical bar of length ℓ and radius r. On this bar must be placed a winding which will produce a specified output voltage for a specified ambient magnetic field which is varying with time.

The ambient magnetic field will be assumed uniform in space and sinusoidal in time.

$$h = H_o \sin \omega t \tag{A. 1}$$

It will also be assumed that the flux density in the bar is independent of the radius and given by the relationship

$$B = \mu_o \mu h, \tag{A. 2}$$

where μ_o is free-space permeability

μ is relative permeability of the bar at a particular axial location.

If the flux in air is neglected, the voltage induced in a single turn of wire around the core will be

$$e = \frac{d}{dt} \phi = \left[\frac{d}{dt} (\mu H_o \sin \omega t) \right] \mu_o A, \tag{A. 3}$$

where A is the area of the core.

Although the relative permeability is a function of flux density, and hence a function of time, this will be neglected by assuming that μ is an

effective value of relative permeability which is known at the location of each turn of wire.

Fig. 2a shows the bar of length ℓ and radius r and the outline of one-half of a symmetrical winding specified by f(x). The radius r_1 includes the coil form thickness. The radius r_1' is the mean radius of the smallest turn of wire.

Fig. 2b shows the allowance for spacing between turns, K_1 and K_2 being dimensionless.

Fig. 2c shows the variation of relative permeability $\mu(x)$ along the bar, using the same origin as for f(x), that is, the mid-point of the bar.

Rewriting Eq. (A. 3) at x_j,

$$e_j = \omega \mu_o H_o A \mu(x_j) \cos \omega t, \tag{A. 4}$$

or

$$E_j = K \mu(x_j), \quad K = \frac{\omega \mu_o H_o A}{\sqrt{2}} \tag{A. 5}$$

Eq. (A. 5) gives the rms voltage induced in one turn at the point x_j along the rod from its mid-point. Assuming that any turn located at x_j will produce the emf E_j, the total emf produced at x_j is

$$T_j K \mu(x_j),$$

where T_j is the number of turns stacked radially. Summing along the length of the bar, the voltage produced by both halves of the winding is

$$E = 2K \sum_{j=1}^{n} T_j \mu(x_j). \tag{A. 6}$$

But the numbers n and T_j are functions of wire diameter and spacing,

$$T_j = \left[\frac{f(x_j)}{K_1 d} \right] \tag{A.7}$$

$$n = \left[\frac{C}{K_2 d} \right] \tag{A.8}$$

where the brackets denote least integer. If it is assumed that f(x) just covers the winding at all points, that is, that no parts of the fractions appearing in Eqs. (A.7) and (A.8) are discarded, the summation is then

$$\sum_{j=1}^{n} T_j \mu(x_j) = \frac{n}{C} \int_o^c T \mu \, dx, \tag{A.9}$$

and the total voltage is

$$E = \frac{2K}{C} \left(\frac{C}{K_2 d} \right) \int_o^c \frac{f(x)}{K_1 d} \mu(x) \, dx,$$

$$E = \frac{2K}{K_1 K_2 d^2} \int_o^c f(x) \mu(x) \, dx, \tag{A.10}$$

or solving for d^2,

$$d^2 = \frac{2K}{E K_1 K_2} \int_o^c f(x) \mu(x) \, dx,$$

$$d^2 = \frac{\int_o^c f \mu \, dx}{K_1 K_2 K'}, \quad K' = \frac{E}{\sqrt{2} \omega \mu_o H_o A}. \tag{A.11}$$

Eq. (A.11) specifies the wire diameter for a required rms output voltage (open-circuit).

The length of the wire will be considered next. At any x_j the length is

$$\phi_j = 2\pi \left\{ r_1' + (r_1' + K_1 d) + (r_1' + 2K_1 d) + \ldots + [r_1' + (T_j - 1) K_1 d] \right\}$$

$$\phi_j = 2\pi \left[T_j r_1' + K_1 d \sum_{a=1}^{T_j} (a - 1) \right]. \qquad \text{(A. 12)}$$

The summation in Eq. (A. 12) can be represented by the parabolic equation

$$\sum_{a=1}^{T_j} (a - 1) = \frac{T_j}{2} (T_j - 1). \qquad \text{(A. 13)}$$

Using Eq. (A. 7) and the assumption of Eq. (A. 9),

$$\sum_{a=1}^{T_j} (a - 1) = \frac{f(x_j)}{2 K_1 d} \left[\frac{f(x_j)}{K_1 d} - 1 \right], \qquad \text{(A. 14)}$$

and the length at x_j is

$$\phi_j = 2\pi \left\{ \frac{f(x_j)}{K_1 d} r_1' + \frac{f(x_j)}{2} \left[\frac{f(x_j)}{K_1 d} - 1 \right] \right\}$$

$$\phi_j = \frac{2\pi}{K_1 d} \left\{ \frac{f^2(x_j)}{2} + f(x_j) \left[r_1' - \frac{K_1 d}{2} \right] \right\}$$

$$\phi_j = \frac{2\pi}{K_1 d} \left[\frac{f^2(x_j)}{2} + r_1 f(x_j) \right]. \qquad \text{(A. 15)}$$

The total wire length is then

$$\phi = 2 \sum_{j=1}^{n} \phi_j + \phi_A, \qquad \text{(A. 16)}$$

in which ϕ_A is the additional wire length required to connect turns and to connect layers. Using Eq. (A. 8),

$$\phi = \phi_A + 2\left(\frac{c}{K_2 d}\right)\left(\frac{2\pi}{K_1 d}\right)\frac{1}{C}\int_0^C \left[\frac{f^2(x)}{2} + r_1 f(x)\right] dx,$$

$$\phi = \phi_A + \frac{4\pi}{K_1 K_2 d^2}\int_0^C \left[\frac{f^2(x)}{2} + r_1 f(x)\right] dx. \qquad \text{(A. 17)}$$

APPENDIX B

The Parabolic Winding

The basic equations for wire diameter and wire length, Eqs. (A.11) and (A.17), are repeated here in slightly different form.

$$K_1 K_2 d^2 K' = \int_0^c f(x)\mu(x)\,dx, \quad K' = \frac{E}{\sqrt{2}\,\omega\mu_o H_o A}, \tag{B.1}$$

$$\frac{K_1 K_2 d^2 \phi}{4\pi} = \frac{1}{2}\int_0^c f^2(x)\,dx + r_1\int_0^c f(x)\,dx, \tag{B.2}$$

where ϕ_A has been neglected in Eq. (B.2).

Let the thickness of the winding be specified by

$$f(x) = H\left[1 - J\left(\frac{x}{c}\right)^2\right], \tag{B.3}$$

where H is the thickness at the center of the winding and J is a dimensionless shaping factor (see Fig. 2a). Since f(x) must be positive, J has a maximum value of one. For this value, the winding has zero thickness on the ends. For J = 0, the winding is cylindrical. And the winding is thicker on the ends than in the center for J < 0.

The permeability function will be taken as

$$\mu(x) = \mu_1\left[1 - F\left(\frac{x}{\ell}\right)^2\right], \tag{B.4}$$

where μ_1 is the effective relative permeability at the center of the bar and F

is a dimensionless constant less than four. The actual value will be assumed to be $F = 3.6$.

The integrals appearing in Eqs. (B.1) and (B.2) can now be evaluated as

$$\int_o^c f^2\,dx = CH\left(1 - \frac{2}{3}J + \frac{J^2}{5}\right), \tag{B.5}$$

$$\int_o^c f\,dx = CH\left(1 - \frac{J}{3}\right), \tag{B.6}$$

$$\int_o^c f\mu\,dx = CH\mu_1\left[\left(1 - \frac{Z^2}{3}\right) - J\left(\frac{1}{3} - \frac{Z^2}{5}\right)\right], \tag{B.7}$$

where $$Z = \sqrt{F}\left(\frac{C}{\ell}\right).$$

Substitution in Eqs. (B.1) and (B.2) yields

$$K_1K_2d^2K' = CH\mu_1\left[\left(1 - \frac{Z^2}{3}\right) - J\left(\frac{1}{3} - \frac{Z^2}{5}\right)\right]$$

and

$$\frac{K_1K_2d^2\phi}{4\pi} = CH\left[\frac{H}{2}\left(1 - \frac{2}{3}J + \frac{J^2}{5}\right) + r_1\left(1 - \frac{J}{3}\right)\right].$$

The quantities C and H are now replaced by

$$C = Z\frac{\ell}{\sqrt{F}}$$

and

$$H = r_1H'. \tag{B.8}$$

$$\frac{K_1 K_2 d^2 \sqrt{F}}{\ell r_1} \left(\frac{K'}{\mu_1}\right) = H'Z \left[\left(1 - \frac{Z^2}{3}\right) - J\left(\frac{1}{3} - \frac{Z^2}{5}\right) \right] \qquad \text{(B.9)}$$

$$\frac{K_1 K_2 d^2 \sqrt{F}\,\phi}{4\pi \ell r_1^2} = H'Z \left[\frac{H'}{2} \left(1 - \frac{2}{3}J + \frac{J^2}{5}\right) + \left(1 - \frac{J}{3}\right) \right] \qquad \text{(B.10)}$$

Since H' can be readily found from Eq. (B.9), its substitution in Eq. (B.10) provides some useful information.

$$\phi = \frac{2\pi \sqrt{F}}{\ell} \left(\frac{K'}{\mu_1}\right)^2 K_1 K_2 d^2 \frac{\left(1 - \frac{2}{3}J + \frac{J^2}{5}\right)}{Z\left[\left(1 - \frac{Z^2}{3}\right) - J\left(\frac{1}{3} - \frac{Z^2}{5}\right) \right]^2}$$

$$+ 4\pi r_1 \left(\frac{K'}{\mu_1}\right) \frac{\left(1 - \frac{J}{3}\right)}{\left[\left(1 - \frac{Z^2}{3}\right) - J\left(\frac{1}{3} - \frac{Z^2}{5}\right) \right]} \qquad \text{(B.11)}$$

Eq. (B.11) can be written in several different forms, a few of which follow:

$$\phi = m_1 (K_1 K_2 d^2) + b_1 \qquad \text{(a)}$$

$$\phi = m_2 E^2 + b_2 E \qquad \text{(b)}$$

$$\phi = \frac{m_3}{\mu_1^2} + \frac{b_3}{\mu_1} \qquad \text{(c)} \qquad \text{(B.12)}$$

$$\phi = m_4 \sqrt{F} + b_4 \qquad \text{(d)}$$

$$\phi = m_5 r_1 + b_5 \qquad \text{(e)}$$

The constants m_i, b_i can be determined by inspection of Eq. (B.11). Other equations might be written; however, when ℓ, A, r_1, and μ_1 are used as variables, their mutual dependence must be considered. In each of the Eqs. (B.12) the coil thickness is a dependent variable which is given by Eq. (B.9).

REFERENCES

1 Richard M. Bozorth, Ferromagnetism, New York, D. Van Nostrand Company, Inc., ©1951, p. 780.

2 F. Brailsford, Magnetic Materials, London, Methuen & Co. Ltd., 1960 (Third ed.), p. 17.

3 Victor E. Legg, "Magnetic Measurements at Low Flux Densities Using the Alternating Current Bridge," The Bell System Technical Journal, Vol. 15, Jan. 1936, pp. 39-62.

4 Simon Ramo and John R. Whinnery, Fields and Waves in Modern Radio, New York, John Wiley & Sons, Inc., 1953 (Second ed.), pp. 240, 245.

5 Richard M. Bozorth and D. M. Chapin, "Demagnetizing Factors of Rods," Journal of Applied Physics, Vol. 13, May 1942, pp. 320-326.

6 Ibid., p. 324.

7 J. Würschmidt, Theorie des Entmagnetizierung Factors und der Scherung von Magnetizierungskurven, Vieweg, Braunschweig, 1925.

8 R. R. Boothe, Jr., B. M. Fannin, and F. X. Bostick, Jr., A Geomagnetic Micropulsation Measuring System Utilizing Air-Core Coils as Detectors, Report No. 115, Electrical Engineering Research Laboratory, The University of Texas, 1 August 1960, pp. 39-40.

9 Francis Glover and Francis J. Heyden, A Survey of Geomagnetism, Monograph No. 16, Georgetown Observatory, Georgetown University, Dec. 1960, pp. 17, 20.

10 Bozorth and Chapin, loc. cit., p. 324.

11 H. Block and J. J. Rietveld, "Inductive Aerials in Modern Broadcast Receivers," Philips Technical Review, Vol. 16, No. 7, Jan. 1955, pp. 181-194.

12 Handbook of Chemistry and Physics, ed. Charles D. Hodgman, Cleveland, Ohio, Chemical Rubber Publishing Co., 1942 (26th ed.), p. 1893.

13 Bozorth and Chapin, loc. cit., p. 321.

14 Bozorth, op. cit., pp. 524-532.

15 K. E. Latimer, "Non-linearity in Magnetic Core Materials at Low Field Strengths," in Soft Magnetic Materials for Telecommunications, ed. C. E. Richards and A. C. Lynch, New York, Interscience Publishers Inc., 1953, pp. 38-50.

16 Bozorth, op. cit., p. 528.

17 Ibid., pp. 613-616.

18 Bozorth and Chapin, loc. cit., pp. 323-326.

19 Ibid., p. 321.

20 Reference Data for Radio Engineers, New York, International Telephone and Telegraph Corporation, ©1956 (Fourth ed.), p. 278.

21 "Allegheny Ludlum Mumetal," Pittsburgh, Pa., Allegheny Ludlum Steel Corporation, Blue Sheet E. M.-12, Edition 8, p. 18.

22 Legg, loc. cit., p. 42.

23 Frederick E. Terman, Radio Engineers Handbook, New York, McGraw-Hill Book Company, Inc., 1943, p. 98.

24 Ibid., p. 101.

Contract Nonr 375(14)

DISTRIBUTION LIST

Addressee	Attn.	No. of copies
ASTIA Arlington Hall Station Arlington 12, Virginia	TIP-Dr	10
Director of Defense Research & Development The Pentagon Washington 25, D.C.	Technical Library Room 3C-128	1
Office of the Chief Signal Officer Department of the Army Washington 25, D.C.	SIGFO-64	1
Engineering and Technical Division Office of the Chief Signal Officer Department of the Army Washington 25, D.C.	SIGET	1
Director of Research U.S. Army Signal Research and Development Laboratories Fort Monmouth, New Jersey		3
Commanding Officer U.S. Army Signal Research and Development Laboratories Fort Monmouth, New Jersey	N. Abbott	1
Administrative Engineer Signal Corps Engineering Laboratory Fort Monmouth, New Jersey		1
Chief of Naval Research Department of the Navy Washington 25, D.C.	Code 427 Code 416	2 1
Director U.S. Naval Research Laboratory Washington 25, D.C.	Code 2000 Code 2027 Code 1360	6 2 1
Chief, Bureau of Ships Department of the U.S. Navy Washington 25, D.C.	Code 337 Code 686	2 2
Chief, Bureau of Aeronautics Department of the U.S. Navy Washington 25, D.C.	EL 50 EL 90	1 1

Bureau of Naval Weapons Dept. of the U. S. Navy Washington 25, D. C.	RRE-3	1
Chief of Naval Operations Frequency Allocation Sect. OP-941Q Room 5E777, The Pentagon Building Washington 25, D. C.		1
Chief of Naval Operations Dept. of the U. S. Navy Washington 25, D. C.	Op 55F Op 413	1 1
Director, ONR Branch Office 346 Broadway New York 13, N. Y.		1
Director, ONR Branch Office The John Crerar Library Building, 10th floor 86 E. Randolph St. Chicago 1, Illinois		1
Chief Scientist ONR Branch Office 1030 Green St (East) Pasadena 1, California		1
Office in Charge, ONR Navy No. 100 - Fleet Post Office New York, N. Y.		1
Commanding Officer U. S. Naval Underwater Sound Laboratory New London, Connecticut		1
Commanding Officer Naval Air Development Center Johnsville, Pennsylvania	AAEL	1
Director Naval Ordnance Laboratory White Oak, Maryland		1
Commander U. S. Naval Ordnance Test Station China Lake, California	Technical Library Code 753	1
Librarian, U. S. Naval Postgraduate School Monterey, California		1
U. S. Naval Electronics Laboratory San Diego 52, California	Library	1

Alderman Library University of Virginia Charlottesville, Virginia	John C. Wyllie	1
Commanding General Hq. USAF Washington 25, D.C.	AC-AS/4:AFDRE	1
Aeronautical Systems Division Deputy for Technology-Avionics Dir. Electromagnetic Warfare & Communications Electromagnetic Environment Branch Propagation Section Wright-Patterson AFB, Ohio	Paul W. Springer ASRNCF-2	1
AF Cambridge Research Laboratories Electronics Research Directorate Office of Aerospace Research L. G. Hanscom Field Bedford, Massachusetts	CRRK CRRI CRRD CRRS	1 1 1 1
AF Cambridge Research Laboratories Office of Aerospace Research Geophysics Research Directorate L. G. Hanscom Field Bedford, Massachusetts		1
Commander AF Office of Scientific Research Washington, D.C.	Dr. Wm. J. Otting, Jr	1
U.S. Weather Bureau Department of Commerce Washington, D.C.	Director, Radar Engineering	1
Boulder Laboratories National Bureau of Standards Boulder, Colorado	Library W. H. Campbell Ionospheric Research and Propagation Division	1 1
Office of Technical Services U.S. Dept. of Commerce Washington 25, D.C.		1
ITT Laboratories 3700 E. Pontiac Street Fort Wayne, Indiana	Mrs. Ann Bley	1
Maurice W. Long Engineering Experiment Station Georgia Institute of Technology Atlanta 13, Georgia		1

Department of EE University of Michigan Ann Arbor, Michigan	Dr. S. S. Atwood	1
Research Laboratory of Electronics M.I.T. Cambridge, Massachusetts	H. Zimmerman	1
Federal Communications Commission Room 2209, New P. O. Bldg. Washington 25, D. C.	Asst. Chief Engineer in Charge of Technical Research Division	1
Stanford Electronics Laboratories Stanford University Stanford, California	Applied Electronics Lab Document Library	1
Library, ERL 427 Corey Hall, University of California Berkeley 4, California	Miss L. Khouri	1
Documents Library R-3446 General Electric Company Missile and Space Vehicle Dept. 3198 Chestnut Street Philadelphia 4, Pa.	Lawrence I. Chasen Mgr., Library	1
Bell Telephone Company P. O. Box 107 Red Bank, New Jersey	Dr. R. Kompfner	1
Dr. William A. Miller Senior Staff Scientist Electronics Systems Division Fairchild Stratas Corp. Straight Path Wyandanch, N. Y.		1
Electrical Engineering Research Labs University of Illinois Urbana, Illinois	P. D. Coleman Room 218	1
RCA Laboratories Princeton, New Jersey	Miss Fern Cloack	1
Technical Reports Collection Gordon McKay Library Harvard University Div. of Eng'g. and Appl. Physics Pierce Hall, Oxford Street Cambridge 38, Mass.	Mrs. Elizabeth Farkas	1
School of Electrical Engineering Cornell University Ithaca, New York	Dr. W. E. Gordon	1

Commandant (EEE) U. S. Coast Guard (Sta 5-5) 1300 E Street, N. W. Washington 25, D. C.		1
M. I. T., Lincoln Laboratory Box 73 Lexington 73, Mass.	Dr. James H. Chisholm	1
Dept. of Electrical Engineering California Institute of Technology Pasadena, California	Dr. C. H. Papas	1
Applied Physics Laboratory The Johns Hopkins University 8621 Georgia Avenue Silver Spring, Maryland	George L. Seielstad	2
New York University Institute of Mathematical Sciences 25 Waverly Place New York 3, N. Y.	Prof. Morris Kline	1
Program Director, Engineering Sciences National Science Foundation Washington 25, D. C.		1
Antenna Research Laboratory Ohio State University Columbus 10, Ohio	Dr. Thomas Tice	1
Tektronix, Inc. P. O. Box 831 Portland 7, Oregon		1
Smyth Research Associates 3555 Aero Court San Diego 11, California	Electronics Branch	1
Cornell Aeronautical Laboratory, Inc. 4455 Genessee Street Buffalo 21, New York	John P. Desmond, Librarian	1
New York University College of Engineering Dept. of Meteorology and Oceanography University Heights New York 53, N. Y.	Prof. W. J. Pierson	1
Dr. Nicholas George 333 Spalding Bldg. California Institute of Technology Pasadena, California		1

Texas A M College College Station, Texas	Dr. Vance Moyer Radar Met. Section	3
Sylvania Electric Products, Inc. P. O. Box 205 Mountain View, California	Miss Katherine Johnson Electronics Defense Lab.	1
Radio Research Laboratories Ministry of Post & Telecommunications Kokubunji Post Office Tokyo, Japan VIA: U. S. Naval Attache for Air Tokyo, Japan	Planning Section	1
Harvard Observatory 60 Garden Street Cambridge 38, Mass.	A. E. Lilley Dept. of Radio Astronomy	1
University of Arizona Tucson, Arizona	Mr. George Savage Inst. of Atmos. Physics	1
Technical Research Group, Inc 2 Aerial Way Syosset, New York	Jerome R. Lurye	1
Loral Electronics Corporation 835 Bronx River Avenue New York 72, N. Y.	W. Honig	1
National Bureau of Standards P. O. Box 299 Boulder, Colorado	Mr. M. C. Thompson	1
Research Laboratory of Electronics Chalmers Institute of Technology Gothenburg, Sweden	Christina Walsh	1
Advanced Research Projects Agency Room 3D 170, The Pentagon Washington 25, D. C.	Lt. Cmdr. D. E. Chandler	1
Alan H. Barrett, Assoc. Prof Room 26-49 M. I. T. Cambridge 39, Mass.		1
Hughes Aircraft Company Communications Division Box 90902 Los Angeles, California		1